

Statistical State Dynamics of Jet–Wave Coexistence in Barotropic Beta-Plane Turbulence

NAVID C. CONSTANTINOU^a

Cyprus Oceanography Center, University of Cyprus, Lefkosia, Cyprus

BRIAN F. FARRELL

Department of Earth and Planetary Sciences, Harvard University, Cambridge, Massachusetts

PETROS J. IOANNOU

Department of Physics, National and Kapodistrian University of Athens, Athens, Greece

(Manuscript received 21 September 2015, in final form 1 March 2016)

ABSTRACT

Jets coexist with planetary-scale waves in the turbulence of planetary atmospheres. The coherent component of these structures arises from cooperative interaction between the coherent structures and the incoherent small-scale turbulence in which they are embedded. It follows that theoretical understanding of the dynamics of jets and planetary-scale waves requires adopting the perspective of statistical state dynamics (SSD), which comprises the dynamics of the interaction between coherent and incoherent components in the turbulent state. In this work, the stochastic structural stability theory (S3T) implementation of SSD for barotropic beta-plane turbulence is used to develop a theory for the jet–wave coexistence regime by separating the coherent motions consisting of the zonal jets together with a selection of large-scale waves from the smaller-scale motions that constitute the incoherent component. It is found that mean flow–turbulence interaction gives rise to jets that coexist with large-scale coherent waves in a synergistic manner. Large-scale waves that would exist only as damped modes in the laminar jet are found to be transformed into exponentially growing waves by interaction with the incoherent small-scale turbulence, which results in a change in the mode structure, allowing the mode to tap the energy of the mean jet. This mechanism of destabilization differs fundamentally and serves to augment the more familiar S3T instabilities in which jets and waves arise from homogeneous turbulence with the energy source exclusively from the incoherent eddy field and provides further insight into the cooperative dynamics of the jet–wave coexistence regime in planetary turbulence.

1. Introduction

A regime in which jets, planetary-scale waves, and vortices coexist is commonly observed in the turbulence of planetary atmospheres, with the banded winds and embedded vortices of Jupiter and the Saturn North Polar vortex constituting familiar examples (Vasavada and Showman 2005; Sánchez-Lavega et al. 2014).

Planetary-scale waves in the jet stream and vortices, such as cutoff lows, are also commonly observed in Earth's atmosphere. Conservation of energy and entropy in undamped 2D turbulence implies continual transfer of energy to the largest available spatial scales (Fjørtoft 1953). This upscale transfer provides a conceptual basis for expecting the largest scales to become increasingly dominant as the energy of turbulence forced at smaller scale is continually transferred to the larger scales. However, the observed large-scale structure in planetary atmospheres is dominated not by incoherent large-scale turbulent motion, as would be expected to result from the incoherent phase relation of Fourier modes in a turbulent cascade, but rather by coherent zonal jets, vortices, and waves of highly specific form. Moreover, the scale of these coherent structures is

^a Current affiliation: Scripps Institution of Oceanography, University of California, San Diego, La Jolla, California.

Corresponding author address: Navid Constantinou, Scripps Institution of Oceanography, University of California, San Diego, 9500 Gilman Drive, 0213, La Jolla, CA 92093-0213.
E-mail: navid@ucsd.edu

distinct from the largest scale permitted in the flow. An early attempt to understand the formation of jets in planetary turbulence did not address the structure of the jet beyond attributing the jet scale to arrest of the incoherent upscale energy cascade at the length scale set by the value of the planetary vorticity gradient and a characteristic flow velocity (Rhines 1975). In Rhines's interpretation, this is the scale at which the turbulent energy cascade is intercepted by the formation of propagating Rossby waves. While this result provides a conceptual basis for expecting zonal structures with spatial scale limited by the planetary vorticity gradient to form in beta-plane turbulence, the physical mechanism of formation, the precise morphology of the coherent structures, and their stability are not addressed by these general considerations.

Our goal in this work is to continue development of a general theory for the formation of finite-amplitude structures in planetary turbulence, specifically addressing the regime in which jets and planetary waves coexist. This theory identifies specific mechanisms responsible for formation and equilibration of coherent structures in planetary turbulence. A number of mechanisms have been previously advanced to account for jet, wave, and vortex formation. One such mechanism that addresses exclusively jet formation is vorticity mixing by breaking Rossby waves leading to homogenization of potential vorticity (PV) in localized regions (Baldwin et al. 2007; Dritschel and McIntyre 2008), resulting in the case of barotropic beta-plane turbulence in broad retrograde parabolic jets and relatively narrow prograde jets with associated staircase structure in the absolute vorticity. While PV staircases have been obtained in some numerical simulations of strong jets (Scott and Dritschel 2012), vorticity mixing in the case of weak to moderately strong jets is insufficient to produce a prominent staircase structure. Moreover, jets have been shown to form as a bifurcation from homogeneous turbulence, in which case the jet is perturbative in amplitude and wave breaking is not involved (Farrell and Ioannou 2003, 2007).

Equilibrium statistical mechanics has also been advanced to explain formation of coherent structures [e.g., by Miller (1990) and Robert and Sommeria (1991)]. The principle is that dissipationless turbulence tends to produce configurations that maximize entropy while conserving both energy and enstrophy. These maximum entropy configurations in beta-plane turbulence assume the coarse-grained structure of zonal jets (cf. Bouchet and Venaille 2012). However, the relevance of these results to the formation, equilibration, and maintenance of jets in strongly forced and dissipated planetary flows remains to be established.

Zonal jets and waves can also arise from modulational instability (Lorenz 1972; Gill 1974; Manfroi and Young

1999; Berloff et al. 2009; Connaughton et al. 2010). This instability produces spectrally nonlocal transfer to the unstable structure from forced waves and therefore presumes a continual source of waves with the required form. In baroclinic flows, baroclinic instability has been advanced as the source of these waves (Berloff et al. 2009). From the broader perspective of the statistical state dynamics theory used in this work, modulational instability is a special case of a stochastic structural stability theory (S3T) (Parker and Krommes 2014; Parker 2014; Bakas et al. 2015). However, modulational instability does not include the mechanisms for realistic equilibration of the instabilities at finite amplitude, although a Landau-type term has been used to produce equilibration of the modulational instability (cf. Manfroi and Young 1999).

Another approach to understanding the jet-wave coexistence regime is based on the idea that jets and waves interact in a cooperative manner. Such a dynamic is suggested, for example, by observations of a prominent wavenumber-5 disturbance in the Southern Hemisphere (Salby 1982). Using a zonally symmetric two-layer baroclinic model, Cai and Mak (1990) demonstrated that storm-track organization by a propagating planetary-scale wave resulted in modulation in the distribution of synoptic-scale transients configured on average to maintain the organizing planetary-scale wave. The symbiotic forcing by synoptic-scale transients that, on average, maintains planetary-scale waves was traced to barotropic interactions in the studies of Robinson (1991) and Qin and Robinson (1992). While diagnostics of simulations such as these are suggestive, comprehensive analysis of the essentially statistical mechanism of the symbiotic regime requires obtaining solutions of the statistical state dynamics underlying it, and indeed the present work identifies an underlying statistical mechanism by which transients are systematically organized by a planetary-scale wave so as to, on average, support that planetary-scale wave in a spectrally nonlocal manner.

S3T provides a statistical state dynamics (SSD)-based theory accounting for the formation, equilibration, and stability of coherent structures in turbulent flows. The underlying mechanism of jet and wave formation revealed by S3T is the spectrally nonlocal interaction between the large-scale structure and the small-scale turbulence (Farrell and Ioannou 2003). S3T is a non-equilibrium statistical theory based on a closure comprising the nonlinear dynamics of the coherent large-scale structure together with the consistent second-order fluxes arising from the incoherent eddies. The S3T system is a cumulant expansion of the turbulence dynamics closed at second order (cf. Marston et al.

2008), which has been shown to become asymptotically exact for large-scale jet dynamics in turbulent flows in the limit of zero forcing and dissipation and infinite separation between the time scales of evolution of the large-scale jets and the eddies (Bouchet et al. 2013; Tangarife 2015). S3T has been employed to understand the emergence and equilibration of zonal jets in planetary turbulence in barotropic flows on a beta plane and on the sphere (Farrell and Ioannou 2003, 2007, 2009a; Marston et al. 2008; Srinivasan and Young 2012; Marston 2012; Constantinou et al. 2014; Bakas and Ioannou 2013b; Tobias and Marston 2013; Parker and Krommes 2014), in baroclinic two-layer turbulence (Farrell and Ioannou 2008, 2009c), in the formation of dry convective boundary layers (Ait-Chaalal et al. 2016), and in drift-wave turbulence in plasmas (Farrell and Ioannou 2009b; Parker and Krommes 2013). It has been used in order to study the emergence and equilibration of finite-amplitude propagating nonzonal structures in barotropic flows (Bakas and Ioannou 2013a, 2014; Bakas et al. 2015) and the dynamics of blocking in two-layer baroclinic atmospheres (Bernstein and Farrell 2010). It has also been used to study the role of coherent structures in the dynamics of the 3D turbulence of wall-bounded shear flows (Farrell and Ioannou 2012; Thomas et al. 2014, 2015; Farrell et al. 2015, manuscript submitted to *J. Fluid Mech.*).

In certain cases, a barotropic S3T homogeneous turbulent equilibrium undergoes a bifurcation in which nonzonal coherent structures emerge as a function of turbulence intensity prior to the emergence of zonal jets, and when zonal jets emerge a new type of jet-wave equilibrium forms (Bakas and Ioannou 2014). In this paper, we use S3T to further examine the dynamics of the jet-wave coexistence regime in barotropic beta-plane turbulence. To probe the jet-wave-turbulence dynamics in more depth, a separation is made between the coherent jets and large-scale waves and the smaller-scale motions, which are considered to constitute the incoherent turbulent component of the flow. This separation is accomplished using a dynamically consistent projection in Fourier space. By this means, we show that jet states maintained by turbulence may be unstable to emergence of nonzonal traveling waves and trace these unstable eigenmodes to what would, in the absence of turbulent fluxes, have been damped wave modes of the mean jet. Thus, we show that the cooperative dynamics between large-scale coherent and small-scale incoherent motion is able to transform damped modes into unstable modes by altering the mode structure, allowing it to tap the energy of the mean jet.

In this work, we also extend the S3T stability analysis of homogeneous equilibria (Farrell and Ioannou 2003,

2007; Srinivasan and Young 2012; Bakas and Ioannou 2013a,b, 2014; Bakas et al. 2015) to the S3T stability of jet equilibria. We present new methods for the calculation of the S3T stability of jet equilibria, extending the work of Farrell and Ioannou (2003) and Parker and Krommes (2014), which was limited to the study of the S3T stability of jets only with respect to zonal perturbations, to the S3T stability of jets to nonzonal perturbations.

2. Formulation of S3T dynamics for barotropic beta-plane turbulence

Consider a nondivergent flow $\mathbf{u} = (u, v)$ on a beta plane with coordinates $\mathbf{x} = (x, y)$, in which x is the zonal direction and y is the meridional direction, and with the flow confined to a periodic channel of size $2\pi L \times 2\pi L$. The velocity field can be obtained from a streamfunction ψ as $\mathbf{u} = \hat{\mathbf{z}} \times \nabla\psi$, with $\hat{\mathbf{z}}$ the unit vector normal to the x - y plane. The component of vorticity normal to the plane of motion is $\zeta \stackrel{\text{def}}{=} \partial_x v - \partial_y u$ and is given as $\zeta = \Delta\psi$, with $\Delta \stackrel{\text{def}}{=} \partial_x^2 + \partial_y^2$ the Laplacian operator. In the presence of dissipation and stochastic excitation, the vorticity evolves according to

$$\partial_t \zeta = -\mathbf{u} \cdot \nabla \zeta - \beta v - r\zeta + \nu \Delta \zeta + \sqrt{\varepsilon} \xi, \quad (1)$$

in which the flow is damped by Rayleigh dissipation with coefficient r and viscous dissipation with coefficient ν . The stochastic excitation maintaining the turbulence $\xi(\mathbf{x}, t)$ is a Gaussian random process that is temporally delta correlated with zero mean.

Equation (1) is nondimensionalized using length scale L and time scale T . The double-periodic domain becomes $2\pi \times 2\pi$, and the nondimensional variables in (1) are $\zeta^* = \zeta/T^{-1}$, $\mathbf{u}^* = \mathbf{u}/(LT^{-1})$, $\xi^* = \xi/(L^{-1}T^{-1/2})$, $\varepsilon^* = \varepsilon/(L^2 T^{-3})$, $\beta^* = \beta/(LT)^{-1}$, $r^* = r/T^{-1}$, and $\nu^* = \nu/(L^2 T^{-1})$, where asterisks denote nondimensional units. Hereinafter, all variables are assumed nondimensional, and the asterisk is omitted.

We review now the formulation of the S3T approximation to the SSD of (1). The S3T dynamics was introduced in the matrix formulation by Farrell and Ioannou (2003). Marston et al. (2008) showed that S3T comprises a canonical second-order closure of the exact statistical state dynamics and derived it alternatively using the Hopf formulation. Srinivasan and Young (2012) obtained a continuous formulation that facilitates analytical explorations of S3T stability of turbulent statistical equilibria.

An averaging operator by which mean quantities are obtained, denoted by angle brackets, is required in order to form the S3T equations. Using this averaging operator, the vorticity of the flow is decomposed as

$$\zeta = Z + \zeta', \tag{2}$$

where

$$Z(\mathbf{x}, t) \stackrel{\text{def}}{=} \langle \zeta(\mathbf{x}, t) \rangle \tag{3}$$

is the mean field or the first cumulant of the vorticity and, similarly, for the derived flow fields (i.e., \mathbf{u}, ψ). The example, for example, ζ , satisfy the important property that

$$\langle \zeta' \rangle = 0, \tag{4}$$

which relies on the averaging operation satisfying the Reynolds condition (cf. [Ait-Chaalal et al. 2016](#)) that, for any two fields f and g ,

$$\langle \langle f \rangle g \rangle = \langle f \rangle \langle g \rangle. \tag{5}$$

The equation for the first cumulant is obtained by averaging (1), which after repeated use of (5) becomes

$$\partial_t Z + \mathbf{U} \cdot \nabla Z + \beta V + rZ - \nu \Delta Z = -\nabla \cdot \langle \mathbf{u}' \zeta' \rangle, \tag{6}$$

in which we have assumed $\langle \xi \rangle = 0$. The term $-\nabla \cdot \langle \mathbf{u}' \zeta' \rangle$ represents the source of mean vorticity arising from the eddy vorticity flux divergence.

The second cumulant of the eddy vorticity is the covariance

$$C(\mathbf{x}_a, \mathbf{x}_b, t) \stackrel{\text{def}}{=} \langle \zeta'(\mathbf{x}_a, t) \zeta'(\mathbf{x}_b, t) \rangle, \tag{7}$$

which is a function of five variables: time t and the coordinates of the two points \mathbf{x}_a and \mathbf{x}_b . We write (7) concisely as $C = \langle \zeta'_a \zeta'_b \rangle$.

All second moments of the velocities can be expressed as linear functions of C . For example, the eddy vorticity flux divergence source term, $\nabla \cdot \langle \mathbf{u}'(\mathbf{x}, t) \zeta'(\mathbf{x}, t) \rangle$, in the mean vorticity equation [(6)] can be written as a function of C as follows:

$$\begin{aligned} \nabla \cdot \langle \mathbf{u}' \zeta' \rangle &= \frac{1}{2} \nabla \cdot \langle \mathbf{u}'_a \zeta'_b + \mathbf{u}'_b \zeta'_a \rangle_{a=b} \\ &= \frac{1}{2} \nabla \cdot [\hat{\mathbf{z}} \times (\nabla_a \Delta_a^{-1} + \nabla_b \Delta_b^{-1}) \langle \zeta'_a \zeta'_b \rangle]_{a=b} \\ &= \frac{1}{2} \nabla \cdot [\hat{\mathbf{z}} \times (\nabla_a \Delta_a^{-1} + \nabla_b \Delta_b^{-1}) C]_{a=b} \\ &\stackrel{\text{def}}{=} R(C), \end{aligned} \tag{8}$$

in which $\mathbf{u}'_j \stackrel{\text{def}}{=} \mathbf{u}'(\mathbf{x}_j, t)$ and the subscripts in the differential operators indicate the specific independent spatial variable on which the operator is defined. To derive (8), we made use of $\mathbf{u}' = \hat{\mathbf{z}} \times \nabla \Delta^{-1} \zeta'$, with Δ^{-1} the inverse Laplacian. The notation $a = b$ indicates that the function

of the five independent variables, $\mathbf{x}_a, \mathbf{x}_b$, and t , in (8) is to be considered a function of two independent spatial variables and t by setting $\mathbf{x}_a = \mathbf{x}_b = \mathbf{x}$. By denoting the divergence of the mean of the perturbation vorticity flux $\nabla \cdot \langle \mathbf{u}' \zeta' \rangle$ in (8) as $R(C)$, we underline that the forcing of the mean vorticity equation [(6)] by the eddies depends on the second cumulant (the covariance of the vorticity field). Adopting this notation for the divergence of the mean of the eddy vorticity flux, the equation for the mean vorticity (the first cumulant) [(6)] takes the following form:

$$\partial_t Z + \mathbf{U} \cdot \nabla Z + \beta V + rZ - \nu \Delta Z = -R(C). \tag{9a}$$

The equation for the perturbation vorticity is obtained by subtracting (6) from (1):

$$\begin{aligned} \partial_t \zeta' &= -(\mathbf{U} \cdot \nabla \zeta' + \mathbf{u}' \cdot \nabla Z) - \nabla \cdot (\mathbf{u}' \zeta' - \langle \mathbf{u}' \zeta' \rangle) \\ &\quad - \beta v' - r \zeta' + \nu \Delta \zeta' + \sqrt{\varepsilon} \xi \\ &= A \zeta' - \nabla \cdot (\mathbf{u}' \zeta' - \langle \mathbf{u}' \zeta' \rangle) + \sqrt{\varepsilon} \xi, \end{aligned} \tag{9b}$$

where

$$A \stackrel{\text{def}}{=} -\mathbf{U} \cdot \nabla - [\beta \partial_x - (\Delta \mathbf{U}) \cdot \nabla] \Delta^{-1} - r + \nu \Delta. \tag{10}$$

Using (9b), definition (7), and noting that $\langle \zeta' \rangle = 0$, we obtain the evolution equation for C :

$$\begin{aligned} \partial_t C &= \langle \zeta'_a \partial_t \zeta'_b + \zeta'_b \partial_t \zeta'_a \rangle \\ &= (A_a + A_b) C + \sqrt{\varepsilon} \langle \zeta'_a \xi_b + \zeta'_b \xi_a \rangle \\ &\quad + \langle [\nabla_a \cdot (\mathbf{u}'_a \zeta'_a)] \zeta'_b + [\nabla_b \cdot (\mathbf{u}'_b \zeta'_b)] \zeta'_a \rangle. \end{aligned} \tag{11}$$

Both terms $\langle [\nabla_a \cdot (\mathbf{u}'_a \zeta'_a)] \zeta'_b \rangle$ and $\langle [\nabla_b \cdot (\mathbf{u}'_b \zeta'_b)] \zeta'_a \rangle$ in (11) can be expressed as linear functions of the third cumulant of the vorticity fluctuations, $\Gamma \stackrel{\text{def}}{=} \langle \zeta'_a \zeta'_b \zeta'_c \rangle$, for example,

$$\begin{aligned} \langle [\nabla_a \cdot (\mathbf{u}'_a \zeta'_a)] \zeta'_b \rangle &= \frac{1}{2} \langle \nabla_a \cdot [\mathbf{u}'_a \zeta'_c + \mathbf{u}'_c \zeta'_a]_{c \rightarrow a} \zeta'_b \rangle \\ &= \frac{1}{2} \nabla_a \cdot [\hat{\mathbf{z}} \times (\nabla_a \Delta_a^{-1} + \nabla_c \Delta_c^{-1}) \langle \zeta'_a \zeta'_b \zeta'_c \rangle]_{c \rightarrow a} \\ &= \frac{1}{2} \nabla_a \cdot [\hat{\mathbf{z}} \times (\nabla_a \Delta_a^{-1} + \nabla_c \Delta_c^{-1}) \Gamma]_{c \rightarrow a}, \end{aligned} \tag{12}$$

explicitly revealing that the dynamics of the second cumulant of the eddy vorticity is not closed (notation $c \rightarrow a$ indicates that the function of independent spatial variables $\mathbf{x}_a, \mathbf{x}_b$, and \mathbf{x}_c should be considered a function of only \mathbf{x}_a and \mathbf{x}_b after setting $\mathbf{x}_c \rightarrow \mathbf{x}_a$). The S3T system is obtained by truncating the cumulant expansion at second order either by setting the third cumulant term in

(11) equal to zero or by assuming that the third cumulant term is proportional to a state-independent covariance $Q(\mathbf{x}_a, \mathbf{x}_b)$. The latter is equivalent to representing both the nonlinearity, $\nabla \cdot (\mathbf{u}'\zeta' - \langle \mathbf{u}'\zeta' \rangle)$, and the externally imposed stochastic excitation in (9b) together as a single stochastic excitation $\sqrt{\varepsilon}\xi(\mathbf{x}, t)$ with zero mean and two-point and two-time correlation function:

$$\langle \xi(\mathbf{x}_a, t_1)\xi(\mathbf{x}_b, t_2) \rangle = \delta(t_1 - t_2)Q(\mathbf{x}_a, \mathbf{x}_b), \quad (13)$$

from which it can be shown that¹

$$\langle \zeta'_a \xi_b + \zeta'_b \xi_a \rangle = \sqrt{\varepsilon}Q(\mathbf{x}_a, \mathbf{x}_b), \quad (14)$$

and consequently (11) simplifies to the time-dependent Lyapunov equation:

$$\partial_t C = (A_a + A_b)C + \varepsilon Q. \quad (15)$$

Using parameterization (13) to account for both the eddy–eddy nonlinearity, $\nabla \cdot (\mathbf{u}'\zeta' - \langle \mathbf{u}'\zeta' \rangle)$, and the external stochastic excitation, $\sqrt{\varepsilon}\xi$, implies that full correspondence between the mean equation [(9a)] coupled with the parameterized eddy equation [(9b)] and the nonlinear dynamics [(1)] requires that the stochastic term accounts fully for modification of the perturbation spectrum by the eddy–eddy nonlinearity in addition to the explicit externally imposed stochastic excitation. It follows that the stochastic parameterization required to obtain agreement between the approximate statistical state dynamics and the nonlinear simulations differs from the explicit external forcing alone unless the eddy–eddy interactions are negligible.

The resulting S3T system is an autonomous dynamical system involving only the first two cumulants that determines their consistent evolution. The S3T system for a chosen averaging operator is

$$\partial_t Z = -\mathbf{U} \cdot \nabla Z - \beta V - rZ + \nu \Delta Z - R(C), \quad (16a)$$

$$\partial_t C = (A_a + A_b)C + \varepsilon Q. \quad (16b)$$

For the purpose of studying turbulence dynamics, it is appropriate to choose an averaging operator that isolates the physical mechanism of interest. Typically, the averaging operator is chosen to separate the coherent structures from the incoherent turbulent motions. Coherent structures are critical components of turbulence in shear flow, both in the energetics of interaction between the large and small scales and in the mechanism by which the statistical steady state is determined.

Retaining the nonlinearity and structure of these flow components is crucial to constructing a theory of shear-flow turbulence that properly accounts for the role of the coherent structures. In contrast, nonlinearity and detailed structure information is not required to account for the role of the incoherent motions, and the statistical information contained in the second cumulant suffices to include the influence of these on the turbulence dynamics. This results in a great practical as well as conceptual simplification that allows a theory of turbulence to be constructed. In the case of beta-plane turbulence, a phenomenon of interest is the formation of coherent zonal jets from the background of incoherent turbulence. To isolate the dynamics of jet formation, zonal averaging is appropriate. Alternatively, if the focus of study is the emergence of large planetary-scale waves, the averaging operation would be an appropriate extension of the Reynolds average over an intermediate spatial scale to produce a spatially coarse-grained–fine-grained flow separation. An averaging operation of this form was used by Bernstein and Farrell (2010) in their S3T study of blocking in a two-layer baroclinic atmosphere and by Bakas and Ioannou (2013a, 2014) to provide an explanation for the emergence of traveling wave structures (zonons) in barotropic turbulence. However, the Reynolds average defined over an intermediate time or space scale,

$$\langle f(\mathbf{x}, t) \rangle \stackrel{\text{def}}{=} \frac{1}{2T} \int_{t-T}^{t+T} d\tau f(\mathbf{x}, \tau), \quad (17a)$$

or

$$\langle f(\mathbf{x}, t) \rangle \stackrel{\text{def}}{=} \frac{1}{4XY} \int_{x-X}^{x+X} dx' \int_{y-Y}^{y+Y} dy' f(\mathbf{x}', t), \quad (17b)$$

satisfies the Reynolds condition (5) only approximately and to the extent that there is adequate scale separation. The S3T system that was derived in (16) is exact if the averaging operation is the zonal average and an adequate approximation for jets and a selection of large-scale waves if there is sufficient scale separation to satisfy the Reynolds condition (5).

Because the scale separation assumed in (16) is only approximately satisfied in many cases of interest, an alternative formulation of S3T will now be obtained in which separation into two independent interacting components of different scales is implemented [a similar formulation was independently derived by Marston et al. (2016)]. This formulation makes more precise the dynamics of the coherent jet and wave interacting with the incoherent turbulence regime in S3T.

¹ Assumption (13) implies identity (14) even when ζ' obeys the nonlinear (9b) (cf. Farrell and Ioannou 2016; Constantinou 2015).

The required separation is obtained by projecting the dynamics (1) on two distinct sets of Fourier harmonics. Consider the Fourier expansion of the streamfunction,

$$\psi = \sum_{k_x} \sum_{k_y} \hat{\psi}_{\mathbf{k}} e^{i\mathbf{k}\cdot\mathbf{x}}, \quad (18)$$

with $\mathbf{k} = (k_x, k_y)$ and the projection operator P_K defined as (cf. Frisch 1995)

$$P_K \psi \stackrel{\text{def}}{=} \sum_{|k_x| \leq K} \sum_{k_y} \hat{\psi}_{\mathbf{k}} e^{i\mathbf{k}\cdot\mathbf{x}} \quad (19)$$

so that the large-scale flow is identified through streamfunction $\Psi = P_K \psi$ and the small-scale flow through $\psi' = (I - P_K)\psi$, where

$$(I - P_K)\psi \stackrel{\text{def}}{=} \sum_{|k_x| > K} \sum_{k_y} \hat{\psi}_{\mathbf{k}} e^{i\mathbf{k}\cdot\mathbf{x}}, \quad (20)$$

with I the identity. Similarly, vorticity and velocity fields are decomposed into $\zeta = Z + \zeta'$ and $\mathbf{u} = \mathbf{U} + \mathbf{u}'$.

From (1) and under the assumption that the stochastic excitation projects only on the small scales, the large scales evolve according to

$$\begin{aligned} \partial_t Z = & -P_K[\mathbf{U} \cdot \nabla Z + \nabla \cdot (\mathbf{u}' \zeta')] - P_K(\mathbf{U} \cdot \nabla \zeta' + \mathbf{u}' \cdot \nabla Z) \\ & - \beta V - rZ + \nu \Delta Z, \end{aligned} \quad (21a)$$

while the small scales evolve according to

$$\begin{aligned} \partial_t \zeta' = & -(I - P_K)(\mathbf{U} \cdot \nabla \zeta' + \mathbf{u}' \cdot \nabla Z) \\ & - (I - P_K)[\mathbf{U} \cdot \nabla Z + \nabla \cdot (\mathbf{u}' \zeta')] \\ & - \beta v' - r \zeta' + \nu \Delta \zeta' + \sqrt{\varepsilon} \xi. \end{aligned} \quad (21b)$$

If P_K were an averaging operator that satisfied the Reynolds condition (5), term $P_K(\mathbf{U} \cdot \nabla \zeta' + \mathbf{u}' \cdot \nabla Z)$ in (21a) would vanish. Here it does not, as both of these terms scatter energy to the large scales. However, an energetically closed S3T system for the first two cumulants can be derived by making the quasi-linear (QL) approximation in (21b): that is, neglect the terms $(I - P_K)[\mathbf{U} \cdot \nabla Z + \nabla \cdot (\mathbf{u}' \zeta')]$ that represent projection of the eddy–eddy and large-scale–large-scale interactions on the eddy-flow components and additionally neglect the terms $P_K(\mathbf{U} \cdot \nabla \zeta' + \mathbf{u}' \cdot \nabla Z)$ in the large-scale (21a). These later terms as well as $(I - P_K)(\mathbf{U} \cdot \nabla Z)$ are not of primary importance to the dynamics and in any case vanish with sufficient scale separation. With these terms neglected we obtain the projected QL system:

$$\begin{aligned} \partial_t Z = & -\beta V - rZ + \nu \Delta Z \\ & - P_K[\mathbf{U} \cdot \nabla Z + \nabla \cdot (\mathbf{u}' \zeta')], \end{aligned} \quad (22a)$$

$$\begin{aligned} \partial_t \zeta' = & -(I - P_K)(\mathbf{U} \cdot \nabla \zeta' + \mathbf{u}' \cdot \nabla Z) \\ & - \beta v' - r \zeta' + \nu \Delta \zeta' + \sqrt{\varepsilon} \xi, \end{aligned} \quad (22b)$$

which conserves total energy and enstrophy in the absence of forcing and dissipation. The conservation properties of the full barotropic equations are retained because the typically small terms that have been discarded scatter energy and enstrophy between (21a) and (21b).

Assuming $Z = P_K(\zeta)$ is the coherent flow and $C = \langle \zeta'(\mathbf{x}_a, t) \zeta'(\mathbf{x}_b, t) \rangle$ is the covariance of the incoherent eddies, with the angle brackets indicating an average over forcing realizations, we obtain the corresponding S3T system for the first two cumulants:

$$\partial_t Z = -\beta V - rZ + \nu \Delta Z - P_K[\mathbf{U} \cdot \nabla Z + R(C)] \quad (23a)$$

and

$$\partial_t C = (I - P_{Ka})A_a C + (I - P_{Kb})A_b C + \varepsilon Q. \quad (23b)$$

It can be shown that these equations have the same quadratic conservation properties as the S3T equations in (16) and the full nonlinear equations in (1). Note that, for $K = 0$, this projection formulation reduces to the zonal mean–eddy formulation employed previously to study zonal jet formation (Farrell and Ioannou 2003, 2007; Srinivasan and Young 2012).

3. Specification of the parameters used in this work

Assume that the large-scale phase coherent motions occupy zonal wavenumbers $|k_x| = 0, 1$, and all zonal wavenumbers $|k_x| \geq 2$ represent phase-incoherent motions so that P_K has $K = 1$.

The covariance of the stochastic excitation in (13) is assumed to be spatially homogeneous [i.e., $Q(\mathbf{x}_a, \mathbf{x}_b) = Q(\mathbf{x}_a - \mathbf{x}_b)$] and can be associated with its Fourier power spectrum $\hat{Q}(\mathbf{k})$:

$$Q(\mathbf{x}_a - \mathbf{x}_b) = \int \frac{d^2 \mathbf{k}}{(2\pi)^2} \hat{Q}(\mathbf{k}) e^{i\mathbf{k} \cdot (\mathbf{x}_a - \mathbf{x}_b)}. \quad (24)$$

Unless otherwise indicated, calculations are performed with the anisotropic power spectrum:

$$\hat{Q}(\mathbf{k}) = \frac{(4\pi/N_f)k_x e^{-k^2 d^2}}{k_x / |k_x| - \text{erf}(k_x d)} \sum_{k_f \in K_f} [\delta(k_x - k_f) + \delta(k_x + k_f)], \quad (25)$$

with $k = |\mathbf{k}|$, $d = 0.2$, $K_f = \{2, 3, \dots, 14\}$ the zonal wavenumbers that are forced, and N_f the total number

of excited zonal wavenumbers. This spectrum is biased toward small k_y wavenumbers, consistent with the assumption that the forcing arises from baroclinic growth processes. The spatial excitation covariance $\hat{Q}(\mathbf{k})$ has been normalized so that each k_f injects equal energy and the total energy injection rate is unity: that is, $\hat{Q}(\mathbf{k})$ satisfies²

$$\int \frac{d^2\mathbf{k}}{(2\pi)^2} \frac{\hat{Q}(\mathbf{k})}{2k^2} = 1. \quad (26)$$

With this normalization, the rate of energy injection by the stochastic forcing in (1), (16), (21), (22), and (23) is ε and is independent of the state of the system, because ξ has been assumed temporally delta correlated.

We choose $\beta = 10$, $r = 0.15$, and $\nu = 0.01$ as our parameters. For $L = 1200$ km and $T = 6$ days, these correspond to $\beta = 1.6 \times 10^{-11} \text{ m}^{-1} \text{ s}^{-1}$ and an e -folding time for linear damping of 40 days. The diffusion coefficient $\nu = 0.01$ is chosen so that scales on the order of the grid are damped in one nondimensional time, and it corresponds to an e -folding time for scales on the order of 1000 km (nondimensional wavenumber $k_x = 7$ in our channel) of approximately 400 days. With these parameters, the channel has zonal extent about 7500 km, which corresponds to 1/4 of the latitude circle at 45° , one unit of velocity corresponds to 23 m s^{-1} , and nondimensional $\varepsilon = 1$ corresponds to an energy input rate of $1.03 \times 10^{-5} \text{ W kg}^{-1}$. Simulations presented in this work are performed using a pseudospectral code with $N_x = N_y = 64$ grid points.

4. S3T jet equilibria

Fixed points of the S3T system correspond to statistical equilibria of the barotropic dynamics. We study these statistical equilibria as a function of ε . For all values of ε and all homogeneous stochastic forcings, there exist equilibria that are homogeneous (both in x and y) with

$$\mathbf{U}^h = (0, 0), \quad C^h(\mathbf{x}_a - \mathbf{x}_b) = \varepsilon \int \frac{d^2\mathbf{k}}{(2\pi)^2} \frac{\hat{Q}(\mathbf{k})}{2(r + \nu k^2)} e^{i\mathbf{k} \cdot (\mathbf{x}_a - \mathbf{x}_b)}, \quad (27)$$

² A stochastic term $\sqrt{\varepsilon}\xi$ with spatial covariance given by (13) can be shown to inject average energy per unit area in the fluid at a rate $(L_x L_y)^{-1} \int d^2\mathbf{x} (\psi_\nu \sqrt{\varepsilon}\xi) = \varepsilon [(2\pi)^{-2} \int d^2\mathbf{k} \hat{Q}(\mathbf{k}) / (2k^2)]$. Since dimensional ξ has units $L^{-1} T^{-1/2}$, we obtain from (13) that Q has dimensions L^{-2} ; therefore its Fourier transform \hat{Q} is dimensionless. Hence, (26) is valid for all values of the dimensional parameters.

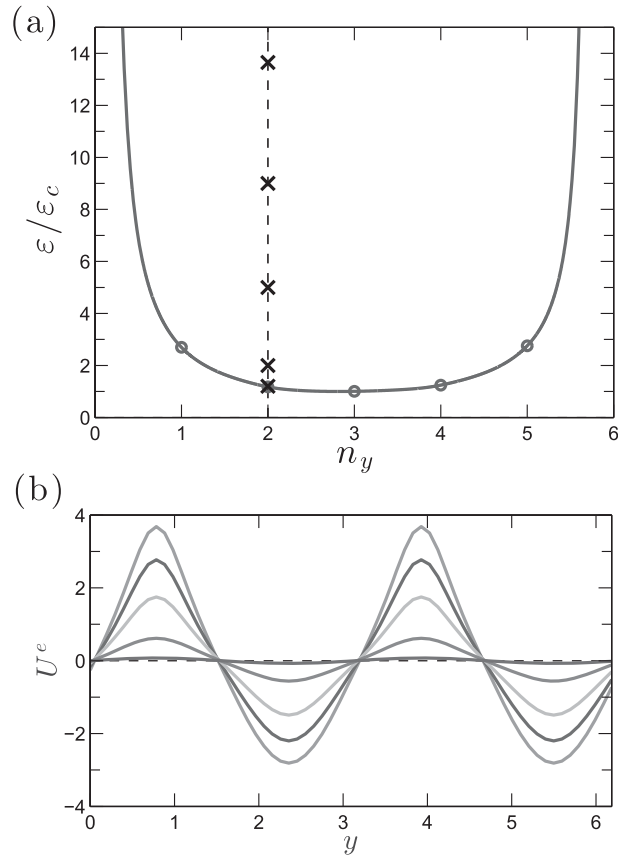


FIG. 1. (a) Normalized turbulent energy input rates $\varepsilon/\varepsilon_c$ at which the homogeneous state becomes unstable to jet ($n_x = 0$) perturbations as a function of the jet meridional wavenumber n_y . Dots indicate wavenumbers allowed in the channel; ε_c is the minimum energy input rate for jet emergence. Jets first emerge in an unrestricted eigencalculation at $\varepsilon_c = 0.2075$ with unallowed wavenumber $n_y = 2.82$. For $\varepsilon/\varepsilon_c < 1.18$, the homogeneous state is stable to $n_y = 2$ mean-flow perturbations and $n_y = 2$ jet equilibria do not exist. (b) The $n_y = 2$ zonal jet S3T equilibrium structure at $\varepsilon/\varepsilon_c = 1.2, 2, 5, 9, 13.65$ [marked with \times in (a)]. Increasing supercriticality results in increasing equilibrium jet amplitude and deviation of the jet structure from the sinusoidal eigenmode form.

where $\hat{Q}(\mathbf{k})$ is the power spectrum of the stochastic forcing, defined in (24).

However, these equilibria become unstable when ε exceeds a critical value. For values of ε exceeding this critical value, zonal jets arise from a supercritical bifurcation (Farrell and Ioannou 2003, 2007; Srinivasan and Young 2012; Parker and Krommes 2013, 2014; Constantinou et al. 2014). These jets are constrained by the periodic domain of our simulations to take discrete values of meridional wavenumber n_y . The critical curve in the ε - n_y plane separating the region in which only stable homogeneous turbulence equilibria exist from the region in which stable or unstable jet equilibria exist is shown, for the chosen parameters, in

Fig. 1. This marginal curve was calculated using the eigenvalue relation for inhomogeneous perturbations to the homogeneous S3T equilibrium in the presence of diffusive dissipation, in the manner of [Srinivasan and Young \(2012\)](#) and [Bakas and Ioannou \(2014\)](#), with the wavenumber n_y taking continuous values but with the understanding that only integer values of n_y satisfy the quantization conditions of the channel. S3T instability of the homogeneous state first occurs at $n_y = 2.82$ for $\varepsilon_c = 0.2075$, which corresponds to $2.15 \times 10^{-6} \text{ W kg}^{-1}$. Jets with $n_y = 3$ emerge at $1.005\varepsilon_c$, and jets with $n_y = 2$ at $1.18\varepsilon_c$. Examples of $n_y = 2$ jet equilibria are shown in [Fig. 1b](#). The $n_y = 2$ jet equilibria have mean flows and covariances that are periodic in y with period $\alpha = \pi$ and satisfy the time-independent S3T equations:

$$\frac{1}{2}[(\partial_{x_a} \Delta_a^{-1} + \partial_{x_b} \Delta_b^{-1})C^e]_{a=b} = rU^e - \nu \partial_y^2 U^e, \quad (28a)$$

$$(A_a^e + A_b^e)C^e = -\varepsilon Q, \quad (28b)$$

with

$$A^e = -U^e \partial_x - [\beta - (\partial_y^2 U^e)] \partial_x \Delta^{-1} - r + \nu \Delta. \quad (29)$$

A basic property of the jet equilibria, which is shared by all S3T equilibria, is that they are hydrodynamically stable (cf. [Farrell and Ioannou 2016](#)). Stability is enforced at the discrete wavenumbers consistent with the finite domain of the problem and not necessarily on the continuum of wavenumbers appropriate for an unbounded domain.

5. S3T stability of the jet equilibria

We are interested in the S3T stability of these $n_y = 2$ jet equilibria to nonzonal perturbations. The stability of jet equilibria to homogeneous in x perturbations has been investigated previously by [Farrell and Ioannou \(2003, 2007\)](#) for periodic domains and by [Parker and Krommes \(2014\)](#) and [Parker \(2014\)](#) for infinite domains. A comprehensive methodology for determining the stability of jet equilibria to zonal and nonzonal perturbations was developed by [Constantinou \(2015\)](#). Recalling these results, perturbations $(\delta Z, \delta C)$ about the equilibrium state (U^e, C^e) , satisfying (28), evolve according to³

$$\partial_t \delta Z = P_K [A^e \delta Z + R(\delta C)], \quad (30a)$$

$$\begin{aligned} \partial_t \delta C = & (I - P_{K_a})(A_a^e \delta C + \delta A_a C^e) \\ & + (I - P_{K_b})(A_b^e \delta C + \delta A_b C^e), \end{aligned} \quad (30b)$$

with R as in (8), A^e defined in (29), and

$$\delta A \stackrel{\text{def}}{=} -\delta \mathbf{U} \cdot \nabla + (\Delta \delta \mathbf{U}) \cdot \nabla \Delta^{-1}, \quad (31)$$

where $\delta \mathbf{U} = \hat{\mathbf{z}} \times \nabla \Delta^{-1} \delta Z$ is the perturbation velocity field.

Because of the homogeneity of the jet equilibria in the zonal (x) direction, the mean-flow eigenfunctions are harmonic functions in x , and also, because the equilibrium mean flow and covariance are periodic in y with period α [i.e., $U^e(y + \alpha) = U^e(y)$], Bloch's theorem requires that each eigenfunction is a plane wave in y ($e^{iq_y y}$) modulated by a periodic function with period α in y ([Cross and Greenside 2009](#); [Parker and Krommes 2014](#)). Therefore, the eigenfunctions take the following form:

$$\delta Z = e^{in_x x + iq_y y + \sigma t} \delta \tilde{Z}_{n_x, q_y}(y), \quad (32a)$$

$$\begin{aligned} \delta C = & e^{in_x(x_a + x_b)/2 + iq_y(y_a + y_b)/2 + \sigma t} [\delta \tilde{C}_{n_x, q_y}(x_a - x_b, y_a, y_b) \\ & + \delta \tilde{C}_{n_x, q_y}(x_b - x_a, y_b, y_a)], \end{aligned} \quad (32b)$$

with $|n_x| \leq K$, $\delta \tilde{Z}_{n_x, q_y}(y)$ periodic in y with period α and $\delta \tilde{C}_{n_x, q_y}(x_a - x_b, y_a, y_b)$ periodic in y_a and y_b with period α . We have chosen δC to be a symmetric function of \mathbf{x} under the exchange $\mathbf{x}_a \leftrightarrow \mathbf{x}_b$.⁴ The zonal wavenumber n_x takes integer values in order to satisfy the periodic boundary conditions in x , and the Bloch wavenumber q_y takes integer values in the interval $|q_y| \leq \pi/\alpha$ in order to satisfy the periodic boundary conditions in y ([Constantinou 2015](#)). The eigenvalue σ determines the S3T stability of the jet as a function of n_x and q_y . The jet is unstable when $\sigma_r \stackrel{\text{def}}{=} \text{Re}(\sigma) > 0$, and the S3T eigenfunction propagates in x with phase velocity $c_r \stackrel{\text{def}}{=} -\text{Im}(\sigma)/n_x$ for $n_x \neq 0$. When $n_x = 0$, the eigenfunctions are homogeneous in the zonal direction and correspond to a perturbation zonal jet. When $n_x \neq 0$, the eigenfunctions are inhomogeneous in both x and y and correspond to a wave. These perturbations, when unstable, can form nonzonal large-scale structures that coexist with the mean flow, as in [Bakas and Ioannou](#)

³These perturbations equations are valid for equilibria inhomogeneous in both x and y directions. In the case of perturbations that are homogeneous in x , the projection operators are redundant.

⁴The covariance eigenfunction does not need to be symmetric or Hermitian in its matrix representation, but both symmetric and asymmetric parts have the same growth rate. For a discussion of the properties of covariance eigenvalue problems see [Farrell and Ioannou \(2002\)](#).

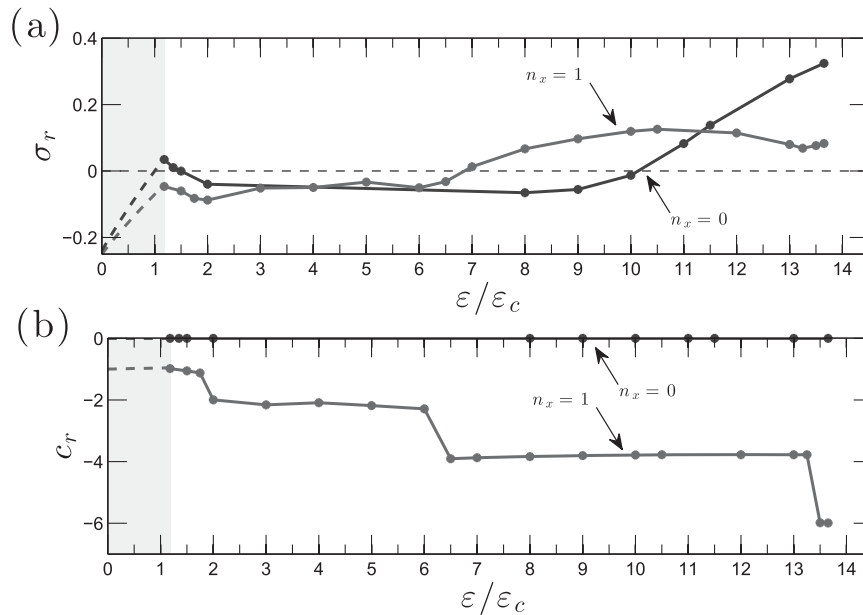


FIG. 2. (a) Maximum S3T growth rates σ_r as a function of $\varepsilon/\varepsilon_c$ for $n_x = 0$ and $n_x = 1$ perturbations to the $n_y = 2$ equilibrium jets. The jet is unstable to $n_x = 0$ perturbations for $1.18 \leq \varepsilon/\varepsilon_c \leq 1.44$ and $\varepsilon/\varepsilon_c \geq 10.14$ and to $n_x = 1$ wave perturbations for $\varepsilon/\varepsilon_c \geq 6.80$. (b) The corresponding phase speeds c_r of the most-unstable S3T eigenfunction.

(2014). For jets with meridional periodicity $\alpha = \pi$, q_y can take only the values $q_y = 0, 1$, and because these jets have a Fourier spectrum with power only at the even wavenumbers, a $q_y = 0$ Bloch eigenfunction has power only at even wavenumbers, while a $q_y = 1$ Bloch eigenfunction has power only at odd wavenumbers.

The maximum growth rate σ_r of the S3T eigenfunction perturbations to the S3T equilibrium jet with $n_y = 2$ (cf. Fig. 1b) is plotted in Fig. 2a as a function of supercriticality $\varepsilon/\varepsilon_c$ for both perturbations of jet form ($n_x = 0$) and nonzonal form (with $n_x = 1$). Consider first the stability of the S3T jet to jet perturbations, that is, to $n_x = 0$ eigenfunctions. Recall that the jets with $n_y = 2$ emerge at $\varepsilon/\varepsilon_c = 1.18$, and for $\varepsilon/\varepsilon_c < 1.18$ (shaded region in Fig. 2a) there are no $n_y = 2$ equilibria. The dashed line shows the smallest decay/fastest growth rate of perturbations to the homogeneous equilibrium state that exists prior to jet formation. The most-unstable eigenfunctions of the homogeneous equilibria at these ε are jets with wavenumber $n_y = 3$ (not shown; cf. Figure 1a). The small-amplitude equilibrated $n_y = 2$ jets that form when ε marginally exceeds the critical $\varepsilon/\varepsilon_c = 1.18$ are unstable to jet formation at wavenumber $n_y = 3$, with jet eigenfunction similar to the maximally growing $n_y = 3$ eigenfunction of the homogeneous equilibrium. This S3T instability of the small-amplitude $n_y = 2$ jet equilibria to $n_y = 3$ jet eigenfunctions, which is induced by the $n_y = 3$ instability of the nearby homogeneous equilibrium, was identified by Parker and Krommes (2014)

as the universal Eckhaus instability of the equilibria that form near a supercritical bifurcation. The Eckhaus unstable S3T $n_y = 2$ jets are attracted to the S3T $n_y = 3$ stable jet equilibrium over the small interval $1.18 < \varepsilon/\varepsilon_c < 1.44$. At higher supercriticalities in the interval $1.44 < \varepsilon/\varepsilon_c < 10.14$, the $n_y = 2$ jets become stable⁵ to $n_x = 0$ eigenfunctions. The jets eventually become unstable to $n_x = 0$ eigenfunctions for $\varepsilon/\varepsilon_c > 10.14$. The most-unstable $n_x = 0$ eigenfunction at $\varepsilon/\varepsilon_c = 11$ is a Bloch $q_y = 1$ eigenfunction, dominated by an $n_y = 1$ jet that will make the jets of the $n_y = 2$ equilibrium merge to form an $n_y = 1$ jet equilibrium (cf. Farrell and Ioannou 2007).

The maximum growth rate of the jet equilibria to $n_x = 1$ nonzonal eigenfunctions is also shown in Fig. 2a. Unlike the jet eigenfunctions, which are stationary with respect to the mean flow, these eigenfunctions propagate retrograde with respect to the jet minimum; the phase velocity of the eigenfunction with maximum real part eigenvalue is plotted as a function of $\varepsilon/\varepsilon_c$ in Fig. 2b. Eigenfunctions with $n_x = 1$ are stable for jets with

⁵ The periodic boundary conditions always allow the existence of a jet eigenfunction with zero growth and with structure that of the y derivative of the equilibrium jet and covariance. This eigenfunction leads to a translation of the equilibrium jet and its associated covariance in the y direction. The existence of this neutral eigenfunction can be verified by taking the y derivative of (28). We do not include this obvious neutral eigenfunction in the stability analysis.

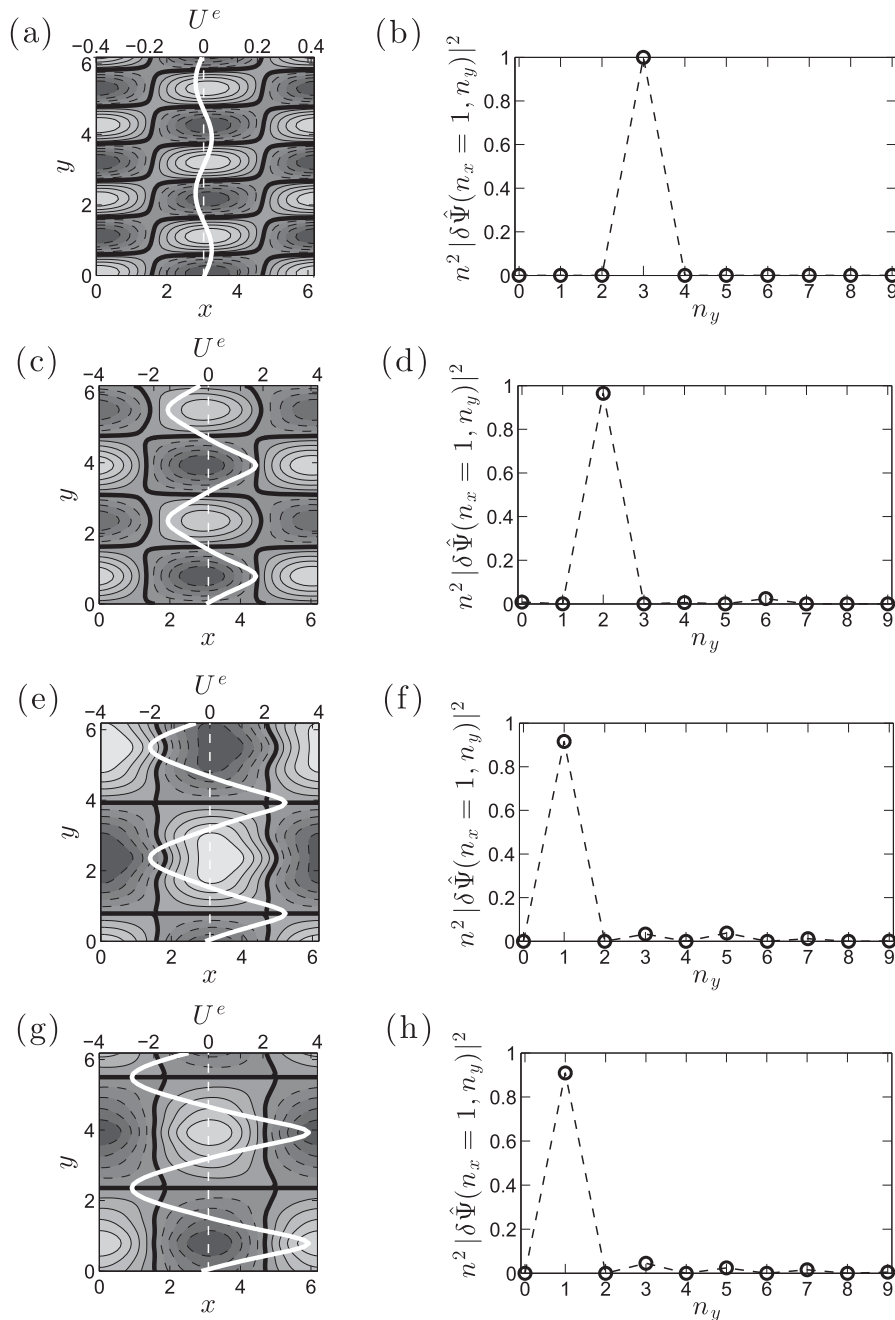


FIG. 3. (a) Contour plot of the streamfunction of the least-stable nonzonal $n_x = 1$ S3T mean-flow wave eigenfunction of the $n_y = 2$ jet equilibrium at $\varepsilon/\varepsilon_c = 1.2$. This wave has growth rate $\sigma_r = -0.047$ and phase speed $c_r = -0.98$. The equilibrium jet is shown in solid white. Positive (negative) contours are indicated with solid (dashed) lines and the zero contour is indicated with a thick solid line. (b) The power spectrum of the mean-flow eigenfunction. This jet equilibrium is unstable to $n_x = 0$ perturbations but stable to $n_x = 1$ perturbations. The least-stable $n_x = 1$ eigenfunction is Bloch $q_y = 1$ with power at $n_y = 3$. (c),(d) As in (a) and (b), respectively, but for the least-stable $n_x = 1$ S3T eigenfunction of the equilibrium at $\varepsilon/\varepsilon_c = 5$. The jet is stable both to $n_x = 0$ and $n_x = 1$ perturbations and the least-stable $n_x = 1$ eigenfunction ($\sigma_r = -0.033$, $c_r = -2.18$) is Bloch $q_y = 0$ with power at $n_y = 2$. (e),(f) As in (a) and (b), respectively, but for the maximally growing $n_x = 1$ S3T eigenfunction of the jet at $\varepsilon/\varepsilon_c = 9$. The jet is stable to $n_x = 0$ perturbations but unstable to $n_x = 1$ perturbations, and the most-unstable $n_x = 1$ eigenfunction ($\sigma_r = 0.099$, $c_r = -3.81$) is Bloch $q_y = 1$ with power at $n_y = 1$. (g),(h) As in (a) and (b), respectively, but for the maximally growing $n_x = 1$ S3T eigenfunction of a strong equilibrium jet at $\varepsilon/\varepsilon_c = 13.65$. The most-unstable $n_x = 1$ eigenfunction ($\sigma_r = 0.083$, $c_r = -5.99$) is Bloch $q_y = 1$ with power at $n_y = 1$. In this case, $n_x = 0$ perturbations are more unstable with $\sigma_r = 0.324$.

$\varepsilon/\varepsilon_c \leq 6.80$, and when they become unstable, the jet is still stable to jet ($n_x = 0$) perturbations. The structures of the least-damped/fastest-growing eigenfunctions at various $\varepsilon/\varepsilon_c$ are shown in Fig. 3. In Figs. 3a and 3b is shown the least-stable eigenfunction of the weak jet at $\varepsilon/\varepsilon_c = 1.2$. The eigenfunction is Bloch $q_y = 1$ with almost all power at $n_y = 3$. The phase velocity of this eigenfunction is $c_r = -0.98$, which is slightly slower than the Rossby phase speed -1 (i.e., $-\beta/k^2$, with $\beta = 10$, $k_x = 1$, $k_y = 3$). In Figs. 3c and 3d is shown the least-stable $n_x = 1$ mode for the jet at $\varepsilon/\varepsilon_c = 5$, which is Bloch $q_y = 0$ with almost all power at $n_y = 2$ and phase speed $c_r = -2.18$, which corresponds to a slightly modified Rossby phase speed with effective PV gradient of $\beta_{\text{eff}} = 10.9$ instead of the $\beta = 10$ of the uniform flow. In Figs. 3e–h are shown the maximally unstable $n_x = 1$ eigenfunctions for the jets at $\varepsilon/\varepsilon_c = 9$ and $\varepsilon/\varepsilon_c = 13.65$. Both are Bloch $q_y = 1$ with almost all power at $n_y = 1$. At $\varepsilon/\varepsilon_c = 9$, the mode is trapped in the retrograde jet, a region of reduced PV gradient, and the structure of this mode as well as its phase speed corresponds, as shown in the next section, to that of an external Rossby wave confined in this equilibrium flow. At $\varepsilon/\varepsilon_c = 13.65$, the eigenfunction is trapped in the prograde jet, a region of high PV gradient, and the structure of this mode as well as its phase speed corresponds to that of an external Rossby wave in this equilibrium flow.

6. The mechanism destabilizing S3T jets to $n_x = 1$ nonzonal perturbations

We now examine the stability properties of the $n_y = 2$ equilibrium jet maintained in S3T at $\varepsilon/\varepsilon_c = 9$. At $\varepsilon/\varepsilon_c = 9$, the jet is stable to $n_x = 0$ jet S3T perturbations but unstable to $n_x = 1$ nonzonal perturbations with maximally growing eigenfunction growth rate $\sigma_r = 0.099$ and phase speed $c_r = -3.806$, which is retrograde at speed 1.61 with respect to the minimum velocity of the jet.

Because the jet U^e is an S3T equilibrium, the operator A^e is necessarily stable to perturbation at zonal wavenumbers that are retained in the perturbation dynamics (i.e., $k_x \in K_f$). The maximum growth rate of operator A^e as a function of k_x for the jet $\varepsilon/\varepsilon_c = 9$ is shown in Fig. 4a, with the integer valued wavenumbers that are included in the S3T dynamics and are responsible for the stabilization of the jet indicated with a circle in this figure. This equilibrium jet, despite its robust hydrodynamic stability at all wavenumbers, in both the mean and eddy equations, and especially its hydrodynamic stability to $n_x = 1$ perturbations, is nevertheless S3T unstable at $n_x = 1$.

Although it is not formed as a result of a traditional hydrodynamic instability, this S3T instability is very close

in structure to the least-stable eigenfunction of A^e at $n_x = 1$, as it can be seen in Figs. 4c and 4d. The spectrum of A^e at $n_x = 1$ is shown in Fig. 4b. The eigenfunctions associated with this spectrum consist of viscous shear modes with phase speeds within the flow and a discrete number of external Rossby waves with phase speeds retrograde with respect to the minimum velocity of the flow (cf. Kasahara 1980). In this case, there are exactly five external Rossby waves with phase speeds $c_r = -3.70, -9.80, -5.92, -2.33,$ and -2.37 , all decaying with $k_x c_i = -0.15, -0.16, -0.17, -0.18,$ and -0.24 , respectively. We identify the S3T $n_x = 1$ unstable eigenfunction, shown in Fig. 4d, which has phase speed $c_r = -3.81$ with S3T destabilization of the least-stable of the external Rossby waves, shown in Fig. 4c, which has phase speed $c_r = -3.70$. This instability arises by Reynolds stress feedback that exploits the least-damped mode of A^e , which is already extracting some energy from the jet through the hydrodynamic instability process, thereby making it S3T unstable. This feedback process transforms a mode of the system that while extracting energy from the mean nevertheless was decaying at a rate $k_x c_i = -0.15$ into an unstable mode growing at rate $\sigma_r = 0.099$. Consistently, note in Fig. 4d that the streamfunction of the S3T eigenfunction is tilting against the shear, indicative of its gaining energy from the mean flow.

We quantify the energetics of the S3T instability in order to examine the instability mechanism in more detail. The contribution to the growth rate of this $n_x = 1$ eigenfunction from interaction with the mean equilibrium jet is

$$\sigma_{10} = \frac{1}{2} \frac{(A_{\text{inv}}(U^e)\delta Z, \delta Z) + (\delta Z, A_{\text{inv}}(U^e)\delta Z)}{(\delta Z, \delta Z)}, \tag{33}$$

where $(f, g) \stackrel{\text{def}}{=} - (2\pi)^{-2} \int d^2\mathbf{x} (1/2) f \Delta^{-1} g$ is the inner product in energy metric, and

$$A_{\text{inv}}(U) = -U\partial_x - [\beta - (\partial_y^2 U)]\partial_x \Delta^{-1} \tag{34}$$

is the inviscid part of (10) with $V = 0$. The contribution to the growth rate of the $n_x = 1$ eigenfunction from Reynolds stress mediated interaction with the small scales is

$$\sigma_{1>} = \frac{1}{2} \frac{(\delta Z, R(\delta C)) + (R(\delta C), \delta Z)}{(\delta Z, \delta Z)}. \tag{35}$$

The net growth rate of the perturbation $n_x = 1$ eigenfunction is then $\sigma_r = \sigma_{10} + \sigma_{1>} + \sigma_{1D}$, with

$$\sigma_{1D} = \frac{1}{2} \frac{(A_D \delta Z, \delta Z) + (\delta Z, A_D \delta Z)}{(\delta Z, \delta Z)}, \tag{36}$$

the loss to dissipation, where

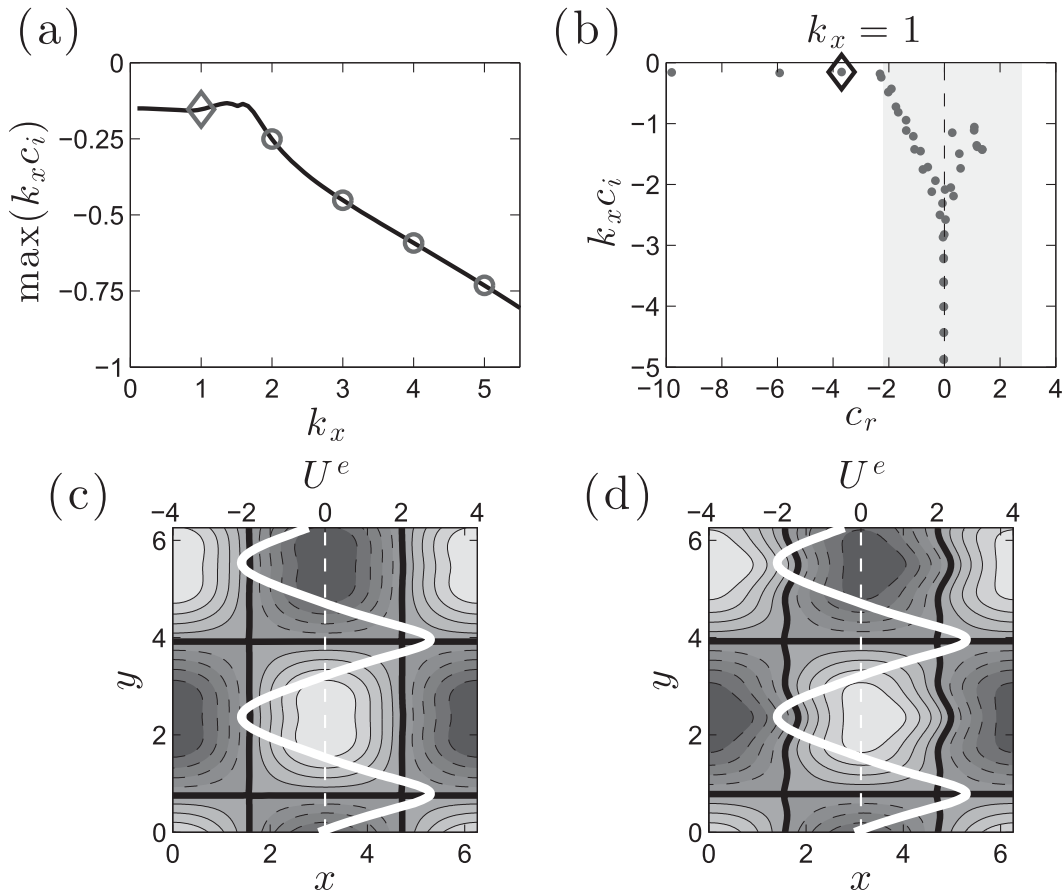


FIG. 4. (a) The hydrodynamic stability of U^e at $\varepsilon/\varepsilon_c = 9$. Shown are the maximal modal growth rates $k_x c_i$ of operator A^e as a function of k_x . Circles indicate the growth rate at the k_x retained in the perturbation dynamics; the diamond indicates the growth rate at $k_x = 1$. The equilibrium jet is hydrodynamically stable but S3T unstable to $n_x = 1$ perturbation. (b) The growth rates $k_x c_i$ and phase speeds c_r of the least-damped eigenvalues of A^e for $k_x = 1$ perturbations. The shaded area indicates the region $\min(U^e) \leq c_r \leq \max(U^e)$. (c),(d) The jet U^e is shown in white. The streamfunction of the maximally growing S3T $n_x = 1$ eigenfunction is shown in (d). This S3T eigenfunction arises from destabilization of the least-damped mode of A^e with $k_x c_i = -0.15$ and $c_r = -3.70$, indicated with the diamond in (b) and shown in (c). The $n_x = 1$ S3T instability with $\sigma_r = 0.099$ and phase speed $c_r = -3.81$ is supported in this case solely by energy transfer from the mean flow U^e (at the rate $\sigma_{10} = 0.303$) against the negative energy transfer from the small-scale perturbation field (at the rate $\sigma_{1>} = -0.016$) and dissipation (at the rate $\sigma_{1D} = -0.188$), with the growth rate of the S3T instability being $\sigma_r = \sigma_{10} + \sigma_{1>} + \sigma_{1D}$.

$$A_D = -r + \nu \Delta \tag{37}$$

is the dissipation part of operator (10).

For the S3T unstable eigenfunction shown in Fig. 4d, the growth rate $\sigma_r = 0.099$ arises solely from interaction with the mean flow, which contributes $\sigma_{10} = 0.303$, while the energy transfer from the small-scale perturbation field contributes negatively, $\sigma_{1>} = -0.016$, with dissipation accounting for the remainder $\sigma_{1D} = -0.188$. Interestingly, this S3T unstable mode is solely supported in its energetics by induced nonnormal interaction with the mean jet and loses energy to the Reynolds stress feedback, which is responsible for the instability. This

remarkable mechanism arises from eddy flux interaction, which transforms damped waves into exponentially growing ones. This is achieved by the Reynolds stresses altering the tilt of the waves so that instead of losing energy to the mean jet, as when they were damped retrograde Rossby waves on the laminar jet, they tap the energy of the mean jet and grow exponentially. This novel mechanism destabilizes the wave even though the direct effect of the Reynolds stresses is to stabilize it. This mechanism of destabilization differs from that acting in more familiar S3T instabilities in which jets and waves arise directly from their interaction with the incoherent eddy field.

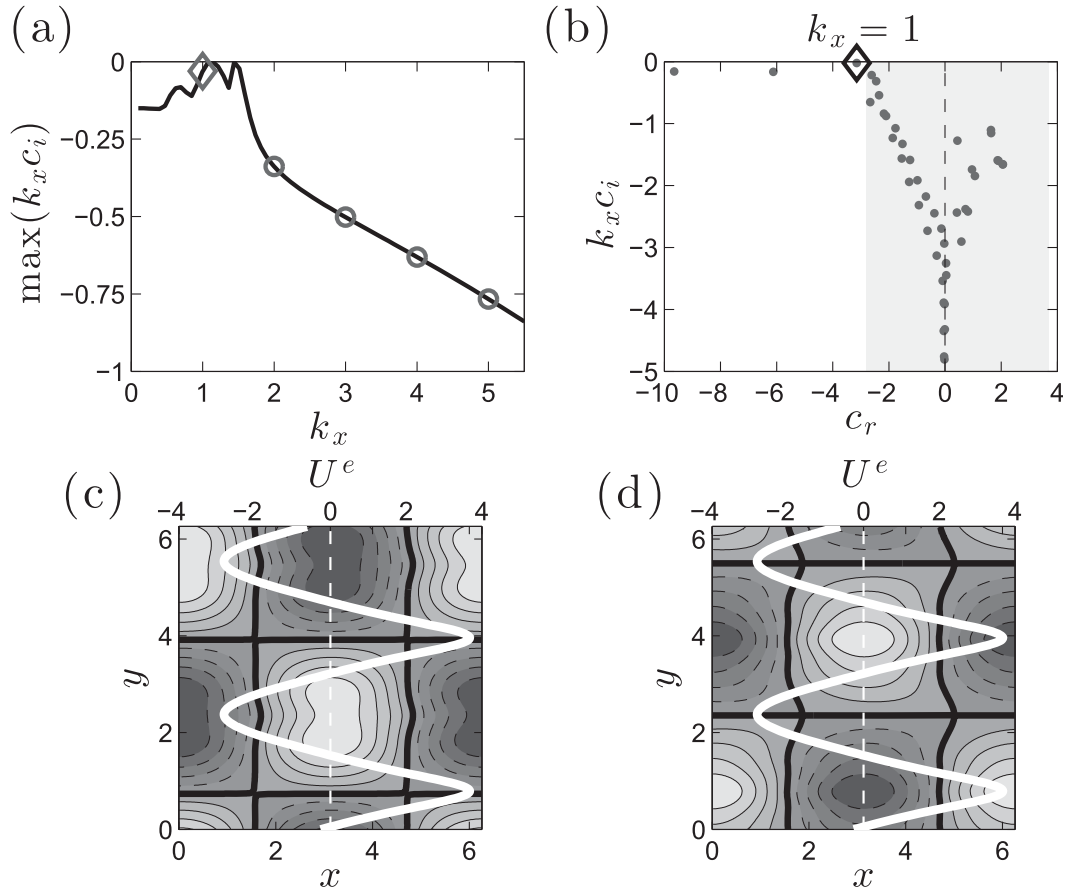


FIG. 5. (a) The hydrodynamic stability of U^e at $\varepsilon/\varepsilon_c = 13.65$. Shown are the maximal modal growth rates $k_x c_i$ of operator A^e as a function of k_x . Circles indicate the growth rate at the k_x retained in the perturbation dynamics; the diamond indicates the growth rate at $k_x = 1$. The equilibrium jet is hydrodynamically stable but S3T unstable to both $n_x = 0$ and $n_x = 1$ perturbations. (b) The growth rates $k_x c_i$ and phase speeds c_r of the least-damped eigenvalues of A^e for $k_x = 1$ perturbations. The shaded area indicates the region $\min(U^e) \leq c_r \leq \max(U^e)$. (c),(d) The jet U^e is shown in white. The streamfunction of the maximally growing S3T $n_x = 1$ eigenfunction is shown in (d). This S3T eigenfunction arises from destabilization of the second-least-damped mode of A^e with $k_x c_i = -0.165$ and $c_r = -6.12$, indicated with a diamond in (b) and shown in (c). The $n_x = 1$ S3T instability with $\sigma_r = 0.083$ and $c_r = -5.99$ is supported in this case by both energy transfer from the mean flow U^e (at the rate $\sigma_{10} = 0.160$) and energy transfer from the small-scale perturbation field (at the rate $\sigma_{1>} = 0.115$). The dissipation rate is $\sigma_{1D} = -0.192$.

This same mechanism is responsible for the S3T destabilization of the $n_x = 1$ perturbation to the jet equilibrium at $\varepsilon/\varepsilon_c = 13.65$. However, at $\varepsilon/\varepsilon_c = 13.65$, the jet is unstable to both $n_x = 0$ (with maximum growth rate $\sigma_r = 0.324$) and to $n_x = 1$ nonzonal perturbations (with maximum growth rate $\sigma_r = 0.083$ and phase speed $c_r = -5.99$, which is retrograde by 3.18 with respect to the minimum velocity of the jet). This equilibrium flow is also hydrodynamically stable at all the zonal wavenumbers allowed by periodicity (cf. Fig. 5a). This $n_x = 1$ unstable eigenfunction (cf. Fig. 5d) arises from destabilization of the second-least-damped mode, which is the damped external Rossby mode indicated in Fig. 5b and shown in Fig. 5c. The energetics of the instability indicate that the growth of this $n_x = 1$ structure arises almost

equally from energy transferred from the mean equilibrium jet to the $n_x = 1$ perturbation ($\sigma_{10} = 0.160$) and energy transferred by the small scales ($\sigma_{1>} = 0.115$), while dissipation accounts for the remainder $\sigma_{1D} = -0.192$.

7. Equilibration of the S3T instabilities of the equilibrium jet

We next examine equilibration of the $n_x = 1$ S3T instability at $\varepsilon/\varepsilon_c = 9$ and the equilibration of the S3T instabilities at $\varepsilon/\varepsilon_c = 13.65$, which has both $n_x = 0$ and $n_x = 1$ unstable eigenfunctions.

Consider the energetics of these large scales consisting of the $k_x = 0$ and $k_x = 1$ Fourier components. Denote the $k_x = 0$ and $k_x = 1$ components of vorticity of (23a) as Z^0

and Z^1 and the corresponding vorticity flux divergence of the incoherent components as R^0 and R^1 and with $Z^e \stackrel{\text{def}}{=} -\partial_y U^e$ the vorticity of the equilibrium zonal jet. The energetics of the equilibration of the S3T instabilities is examined by first removing the constant flux to the large scales from the small scales that maintains the equilibrium flow U^e . For that reason, the vorticity flux divergence associated with the deviation of the instantaneous covariance from C^e will be considered in the equilibration process.

Consider first the energetics of the $k_x = 1$ component of the large-scale flow. The first contribution to the energy growth of this component is the energy transferred from the $k_x = 0$ component of the flow. This occurs at rate

$$\mathcal{E}_{10} = (A_{\text{inv}}(U^0)Z^1, Z^1) + (Z^1, A_{\text{inv}}(U^0)Z^1), \quad (38)$$

with A_{inv} defined in (34) and U^0 the total $k_x = 0$ component of the zonal velocity. The second energy source is energy transferred to $k_x = 1$ from the small scales (i.e., those with $|k_x| > K$), which occurs at rate

$$\mathcal{E}_{1>} = (Z^1, R^1) + (R^1, Z^1), \quad (39)$$

with $R^1 \stackrel{\text{def}}{=} R^1(C - C^e)$ the vorticity flux divergence produced by covariance $C - C^e$. Finally, energy is dissipated at the following rate:

$$\mathcal{E}_{1D} = (A_D Z^1, Z^1) + (Z^1, A_D Z^1), \quad (40)$$

with A_D defined in (37).

The energy flowing to the $k_x = 0$ component consists first of \mathcal{E}_{01} , the energy transfer rate to this component from the $k_x = 1$ component, which is equal to $-\mathcal{E}_{10}$ (being equal and opposite to the energy transfer rate to $k_x = 1$ from the $k_x = 0$ component), and second of the energy transferred to $k_x = 0$ by the small scales, with contribution to the growth rate

$$\mathcal{E}_{0>} = (Z^0, R^0) + (R^0, Z^0), \quad (41)$$

with $R^0 \stackrel{\text{def}}{=} R^0(C - C^e)$. Having removed the energy source sustaining the equilibrium flow, the energy of Z^0 is dissipated at rate

$$\mathcal{E}_{0D} = (A_D(Z^0 - Z^e), Z^0) + (Z^0, A_D(Z^0 - Z^e)). \quad (42)$$

The instantaneous rates of change of the energy of the Z^0 and Z^1 components are then $dE_0/dt = \mathcal{E}_{01} + \mathcal{E}_{0>} + \mathcal{E}_{0D}$ and $dE_1/dt = \mathcal{E}_{10} + \mathcal{E}_{1>} + \mathcal{E}_{1D}$. By dividing each term of dE_1/dt with $2(Z^1, Z^1)$, we obtain, corresponding to (33), (35), and (36), the instantaneous growth rates σ_{10} , $\sigma_{1>}$, and σ_{1D} , and by dividing dE_0/dt with $2(Z^0 - Z^e, Z^0 - Z^e)$, the growth rates σ_{01} , $\sigma_{0>}$, and σ_{0D} . As equilibration is

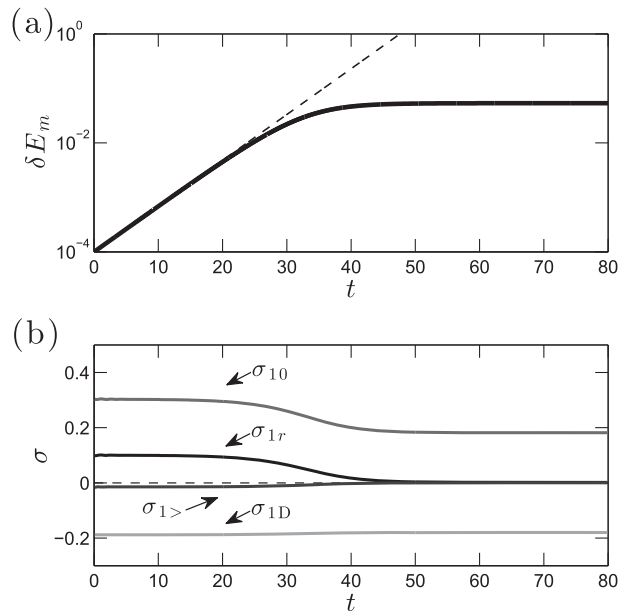


FIG. 6. (a) Evolution of the disturbance energy δE_m of the deviation of the large-scale flow from its zonal equilibrium state at $\varepsilon/\varepsilon_c = 9$ with equilibrium vorticity Z^e . The S3T equilibrium is initially perturbed with the unstable $n_x = 1$ S3T eigenfunction shown in Fig. 4d. Initially, the deviation grows at the predicted exponential growth rate of the eigenfunction (dashed), and the equilibration of this instability produces asymptotically the stationary state shown in Figs. 7a and 7b comprising a jet with a finite-amplitude embedded wave. (b) Evolution of the energetics of the $k_x = 1$ component of the flow. Shown are the contribution to the instantaneous growth rate of $k_x = 1$ by energy transferred from the mean flow σ_{10} , from the small scales $\sigma_{1>}$, and that lost to dissipation σ_{1D} . Also shown is the resulting instantaneous growth rate, $\sigma_{1r} = \sigma_{10} + \sigma_{1>} + \sigma_{1D}$, which necessarily vanishes as equilibration is approached. The S3T instability is supported in this case solely from energy transferred to $k_x = 1$ from U^0 , and equilibration is achieved by reducing this transfer.

approached, the sum of these growth rates approaches zero, while the evolution of the growth rates indicates the role of each energy transfer rate in producing the equilibration.

a. Case 1: $n_x = 1$ instability at $\varepsilon/\varepsilon_c = 9$

Consider first the equilibration of the $n_x = 1$ instability at $\varepsilon/\varepsilon_c = 9$ by first imposing on the jet equilibrium the most-unstable S3T $n_x = 1$ eigenfunction at small amplitude, in order to initiate its exponential growth phase. Evolution of the energy of the Z^1 component of the flow as a function of time, shown in Fig. 6a, confirms the accuracy of our methods for determining the structure and the growth rate of the maximally growing S3T eigenfunction of the jet equilibrium. The contribution of each of the growth rates associated with (38)–(40) to the total normalized energy growth rate of the $k_x = 1$ component of the flow, dE_1/dt , is shown in Fig. 6b. As discussed earlier, the S3T instability is due to the transfer of energy from the zonal flow, and the equilibration is seen

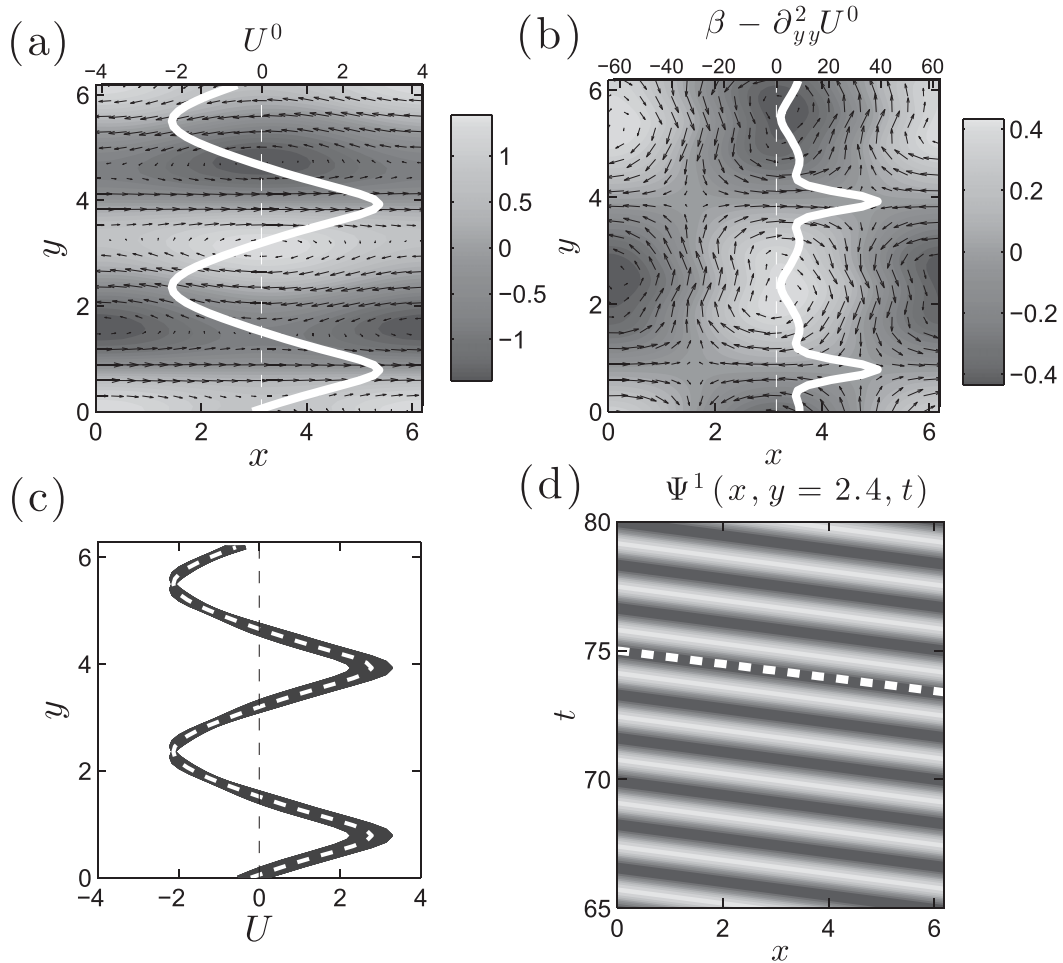


FIG. 7. (a) Mean-flow streamfunction Ψ at $t = 80$, and the velocity field of the $k_x = 0$ and $k_x = 1$ components of the equilibrium at $\varepsilon/\varepsilon_c = 9$ resulting from equilibration of the $n_x = 1$ instability. Also shown in white is U^0 . The equilibrium consists of a jet and a traveling wave that has no critical layer in the flow, as it travels retrograde with respect to the minimum jet velocity. (b) The wave component of the flow Ψ^1 and its associated velocity field. The wave propagates in the retrograde part of the jet where the potential vorticity gradient $\beta - \partial_y^2 U^0$ (white) has a small and nearly constant positive value. (c) Variation of the zonal flow velocity U with y at equilibrium at different x sections. Also shown is U^0 (dashed line), which is nearly identical to the unstable S3T jet U^e . (d) Hovmöller diagram of Ψ^1 at the location of the minimum of U^0 , $y = 2.4$. The phase velocity of the equilibrated wave is equal to the phase speed of the most-unstable S3T eigenfunction (dashed line), shown in Fig. 4d.

to be achieved by reducing the transfer of the energy from the mean flow to the $k_x = 1$ component by reducing the tilt of the nonzonal component of the flow. The Reynolds stress contribution remains approximately energetically neutral. The flow eventually equilibrates to a nearly zonal configuration, which is very close to the initial jet, as shown in Fig. 7c. The equilibrium state, while nearly zonal, contains an embedded traveling wave (cf. Figs. 7a and 7b). This wave propagates westward with phase speed indistinguishable from that of the unstable $n_x = 1$ S3T eigenfunction, as can be seen in the Hovmöller diagram of Ψ^1 , shown in Fig. 7d. The PV gradient of the

equilibrated jet $\beta - \partial_y^2 U^0$ is everywhere positive, and the wave propagates in the retrograde part of jet where the PV gradient is close to uniform. Also, the structure of the nonzonal component of the equilibrated flow is very close to the structure of the most-unstable eigenfunction, as seen by comparing Fig. 4d with Fig. 7b. This equilibrated state is robustly attracting. When the unstable jet is perturbed with random high-amplitude perturbations, the unstable S3T jet is attracted to the same equilibrium. Mixed S3T equilibria of similar form have been found as statistical equilibria of the full nonlinear equations (Bakas and Ioannou 2013a, 2014).

b. Case 2: $n_x = 1$ instability at $\varepsilon/\varepsilon_c = 13.65$

The equilibration of the jet at $\varepsilon/\varepsilon_c = 13.65$ involves the simultaneous equilibration of two S3T instabilities, of the powerful $n_x = 0$ jet instability that grows initially at the rate $\sigma_r = 0.324$ and of the weaker $n_x = 1$ instability that grows initially at rate $\sigma_r = 0.083$. We impose on the equilibrium the most-unstable S3T $n_x = 0$ and $n_x = 1$ eigenfunctions at small but equal amplitudes in order to initiate their exponential growth phases. The evolution of the energy of the $Z - Z^e$ component of the flow as a function of time (cf. Fig. 8a) shows initial growth at the rate of the faster $n_x = 0$ instability. The equilibration process for the $n_x = 0$ instability is shown in Fig. 8b, and the equilibration of the $n_x = 1$ instability in Fig. 8c. The $n_x = 0$ instability is supported by the transfer of energy to the $k_x = 0$ component from the small scales ($\sigma_{0>} > 0$), as is the equilibrated jet. The equilibration of this instability proceeds rapidly and is enforced by reduction of the $\sigma_{0>}$: that is, the transfer of energy from the small scales. During the equilibration process there is a pronounced transient enhancement of the transfer rate to the mean flow by the eddies. This leads to the equilibrated jet shown in Figs. 9a and 9c, which has 5% greater energy than the original S3T unstable equilibrium jet. The equilibrated jet is asymmetric with enhanced power at $n_y = 1$. (In this case, the unstable $n_y = 2$ jet did not merge with the $n_y = 1$ jet to form a jet with a single-jet structure.) During the equilibration process, σ_{01} is always negative, indicating continual transfer of mean jet energy supporting the $n_x = 1$ perturbation. The equilibration of the $n_x = 1$ wave is slower and proceeds in this example, in which the jets did not merge, independently of evolution of the $n_x = 0$ instability. The wave is supported by transfer of energy from the small scales and from transfer of energy from the mean flow. The former remained unaffected during the equilibration process, and equilibration is achieved by reduction of the transfer from the mean flow σ_{10} . The PV gradient of the mean flow, $\beta - \partial_y^2 U^0$, shown in Fig. 9b is positive almost everywhere, and the wave is trapped at the prograde part of the jet. As in the case with $\varepsilon/\varepsilon_c = 9$, the wave propagates at the speed of the S3T eigenfunction (cf. Fig. 9d).

8. Discussion

a. Correspondence between the S3T dynamics (16) and the projected S3T dynamics (23)

Stability of a two-jet state to jet and wave perturbations in the projected S3T formulation (23) is shown in Fig. 2. For parameters for which the base state becomes unstable to nonzonal large-scale perturbations, this base state transitions to a new equilibrium in which the jet coexists with a coherent wave. The stability calculation,

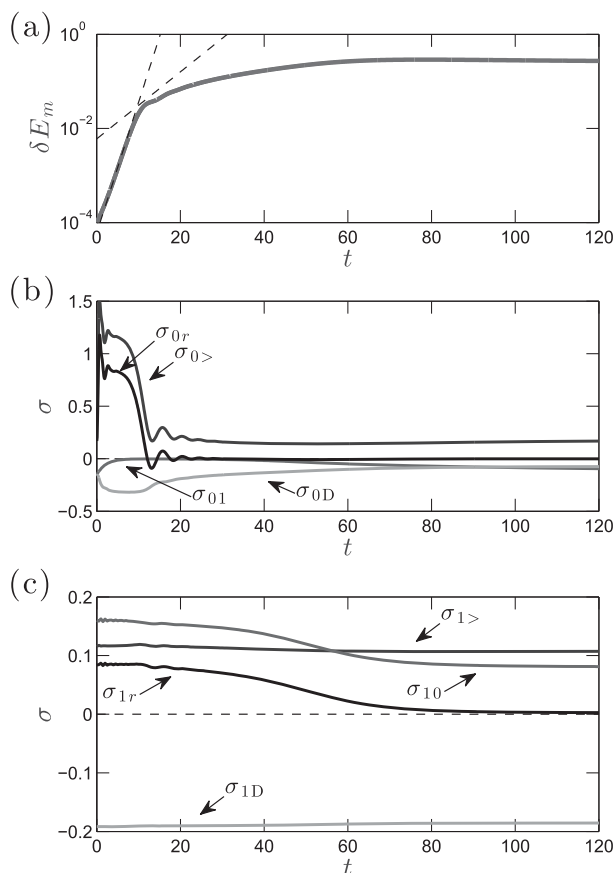


FIG. 8. Evolution of the disturbance energy δE_m associated with the deviation of the large-scale flow $Z - Z^e$, where Z^e is the zonal equilibrium vorticity, at $\varepsilon/\varepsilon_c = 13.65$. The S3T equilibrium is initially perturbed with the unstable $n_x = 0$ and $n_x = 1$ S3T eigenfunctions at small but equal amplitude. The $n_x = 0$ eigenfunction grows at $\sigma_r = 0.324$; the $n_x = 1$ eigenfunction grows at $\sigma_r = 0.083$ (both indicated with dashed lines). Energy grows first at the rate of the $n_x = 0$ instability, up to $t \approx 12$, at which time the equilibration of Z^0 is established. The equilibration of Z^1 is not established until $t \approx 60$. (b) Evolution of the energetics of Z^0 . Shown are the contribution to the instantaneous growth rate of $Z^0 - Z^e$ from energy transferred from Z^1 (σ_{01}), from the small scales ($\sigma_{0>}$), and that lost to dissipation (σ_{0D}). Also shown is the actual instantaneous growth rate σ_{0r} , which vanishes at equilibration. The $n_x = 0$ S3T instability is supported by the transfer of energy from the small scales, and equilibration is achieved rapidly by reducing this transfer. (c) As in (b), but for Z^1 . Shown are the transfer rate from Z^0 (σ_{10}) and from the small scales ($\sigma_{1>}$), as well as the energy dissipation rate (σ_{1D}). The $n_x = 1$ instability is supported by both transfer from Z^0 and from small scales, and the equilibration is established by reducing the transfer from Z^0 .

its energetics, and equilibration process are studied in the framework of the projected S3T equations in (23), which allows a clear separation between the contribution of the coherent jet interaction and that of the incoherent eddies to the instability and equilibration processes. This stability analysis using the projected S3T system produces

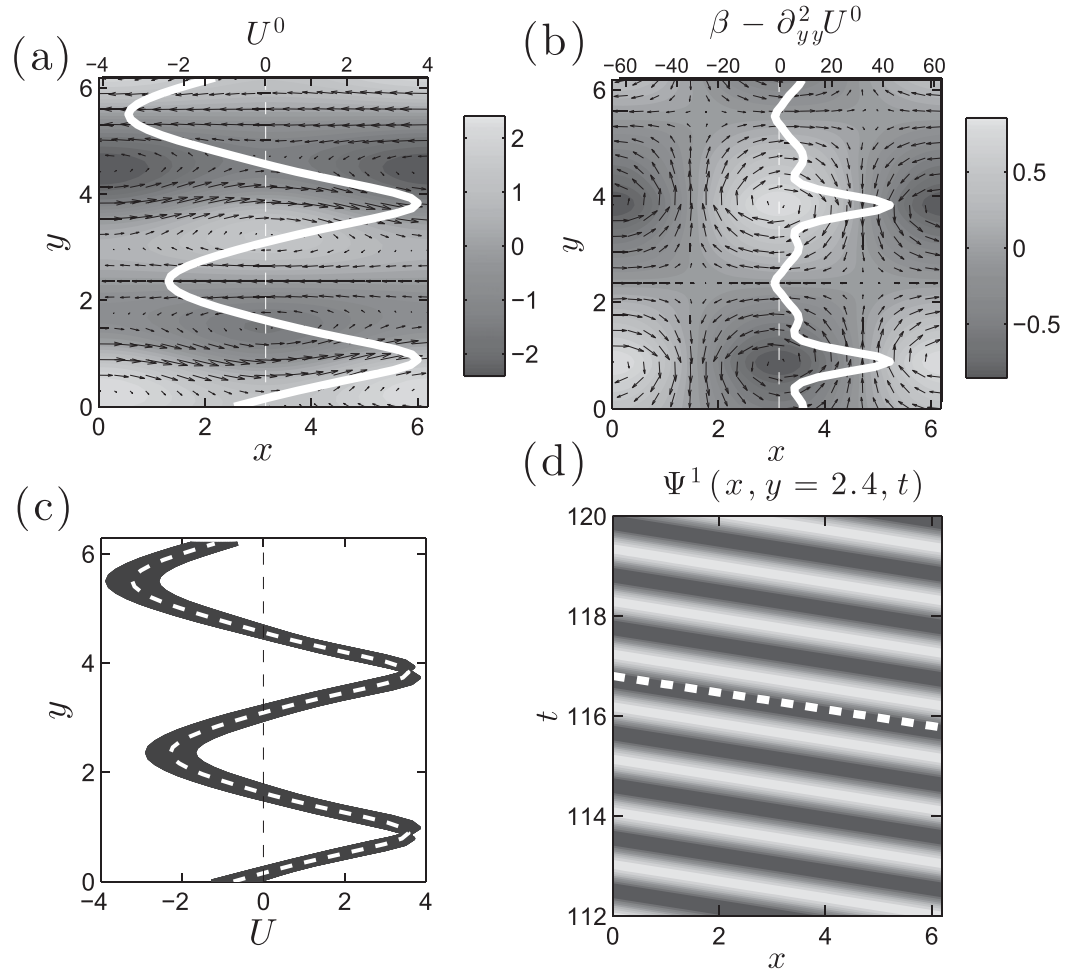


FIG. 9. (a) Mean-flow streamfunction Ψ at $t = 120$, and the velocity field of the $k_x = 0$ and $k_x = 1$ components of the equilibrium at $\varepsilon/\varepsilon_c = 13.65$ resulting from equilibration of both the $n_x = 0$ and $n_x = 1$ instabilities. Also shown in white is U^0 . The equilibrium consists of a jet and a traveling wave that has no critical layer in the flow as it travels retrograde with respect to all U^0 . (b) The wave component of the flow Ψ^1 and its associated velocity field. The wave is trapped in the prograde part of the flow where the potential vorticity gradient (white) is large. (c) Variation of the zonal flow velocity U , with y at equilibrium at different x sections. Also shown is U^0 (dashed line), which is nearly identical to the unstable S3T jet U^e . The equilibrated jet is asymmetric. (d) Hovmöller diagram of Ψ^1 at the location of the zero of U^0 , $y = 1.6$. The phase velocity of the equilibrated wave is equal to the phase speed of the most-unstable S3T eigenfunction (dashed line), shown in Fig. 5d.

essentially the same results as were obtained using the S3T system (16) (cf. Fig. 2 with Figs. 10a,b and Figs. 3e,f with Figs. 10c,d). The equilibrated states produced by these two S3T systems are also very similar (cf. Fig. 11).

b. Reflection of ideal S3T dynamics in QL simulations

The ideal S3T equilibrium jet and the jet–wave states that we have obtained are imperfectly reflected in single realizations of the flow because fluctuations may obscure the underlying S3T equilibrium (cf. Farrell and Ioannou 2003, 2016). The infinite ensemble ideal incorporated

in the S3T dynamics can be approached in the QL [governed by (22)] by introducing in the equation for the coherent flow an ensemble-mean Reynolds stress obtained from a number of independent integrations of the QL eddy equations with different forcing realizations.

Consider, for example, the jet–wave S3T regime at $\varepsilon/\varepsilon_c = 9$ shown in Fig. 7. The energy of the $k_x = 0$ component of the coherent flow is $E_0 = 1.3$ and of the $k_x = 1$ component, which is predominantly a $k_y = 1$ wave, is $E_1 = 0.05$. In Figs. 12a–l is shown the approach of the QL dynamics to this ideal S3T equilibrium as a function of the number of ensemble members N_{ens} , using as

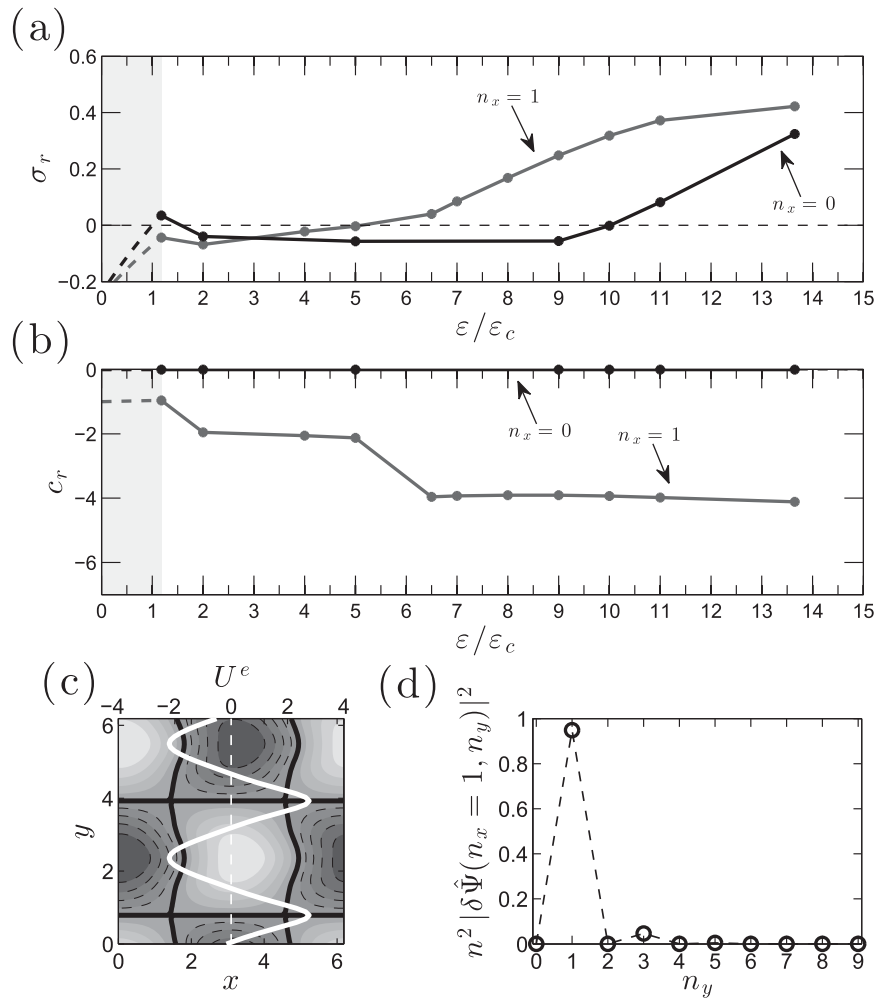


FIG. 10. (a),(b) The stability of the jet equilibria in the S3T formulation (16). The corresponding stability properties of the projected S3T system are shown in Figs. 2a and 2b. (c) Contour plot of the streamfunction of the most-unstable nonzonal $n_x = 1$ S3T mean-flow eigenfunction of the $n_y = 2$ jet equilibrium at $\varepsilon/\varepsilon_c = 9$ with growth rate $\sigma_r = 0.248$ and phase speed $c_r = -3.91$. The equilibrium jet is plotted in solid white. Positive (negative) contours are shown with solid (dashed) lines, and the zero contour is shown with thick solid line. (d) The energy power spectrum of the mean-flow eigenfunction. The jet is stable to $n_x = 0$ perturbations but unstable to $n_x = 1$ perturbations, and the most-unstable $n_x = 1$ eigenfunction is Bloch $q_y = 1$ with power at $n_y = 1$.

diagnostics the structure, indicated by snapshots, of the coherent flow and the energy spectrum. Convergence of the energy of the QL coherent flow components to that of the S3T as N_{ens} increases is shown in Figs. 12m and 12n. These ensemble QL simulations were performed by introducing the mean Reynolds stress divergence obtained from N_{ens} independent simulations of (22b), all with the same large-scale flow, obtained from a single mean QL equation [(22a)]. Convergence to the S3T state is closely approached with $N_{\text{ens}} = 10$. In simulations with a smaller number of ensemble members, the ensemble QL supports an irregular weaker

$k_y = 2$ jet and a stronger $k_x = 1$ coherent flow, which is concentrated at $k_y = 2$ rather than at $k_y = 1$, as predicted in the S3T (cf. Fig. 12b). As the number of ensemble members increases, the jet is more coherently forced, and the ideal S3T $k_x = 1$ component, which was previously masked by fluctuations at $k_y = 2$, is revealed. Also note that in these QL simulations there are no eddy-eddy interactions and also no direct stochastic forcing of the coherent-flow components, and, consequently, their emergence does not result from cascades but from the structural instability mechanisms revealed by S3T.

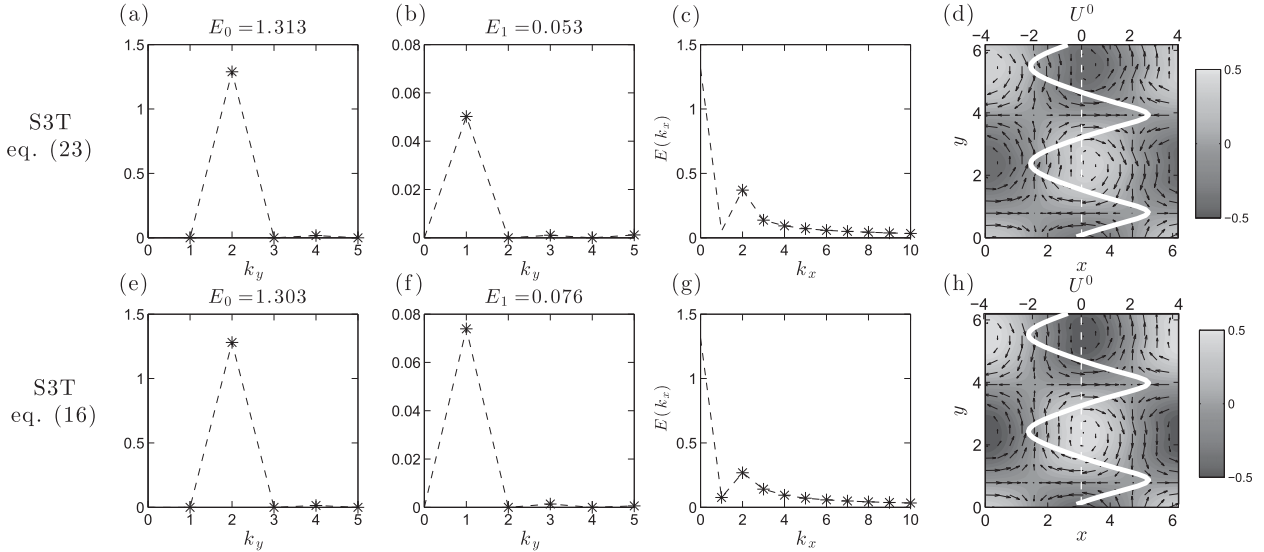


FIG. 11. Comparison of the flows resulting from equilibration of the $n_x = 1$ S3T instabilities of (a)–(d) the projected S3T system (23) and (e)–(h) the S3T system (16) at $\varepsilon/\varepsilon_c = 9$. Shown are the k_y energy spectrum of (a),(e) the mean flow ($k_x = 0$) and (b),(f) $k_x = 1$. (c),(g) The k_x energy spectrum of both the coherent flow components $|k_x| \leq 1$ (circles) and of the incoherent flow components $|k_x| > 1$ (asterisks). (d),(h) Snapshots of the mean jet (thick line) and contour plot of the streamfunction of the $k_x = 1$ wave component.

Both S3T and ensemble simulations isolate and clearly reveal the mechanism by which a portion of the incoherent turbulence is systematically organized by large-scale waves to enhance the organizing wave. However, as in simulation studies revealing this mechanism at work in baroclinic turbulence (Cai and Mak 1990; Robinson 1991), the large-scale wave retains a substantial incoherent component in individual realizations. This is expected in the strongly turbulent atmosphere, considering that even stationary waves at planetary scale, which are strongly forced by topography, are revealed clearly only in seasonal average ensembles.

c. Reflection of ideal S3T dynamics in nonlinear simulations

Consider now the reflection of the S3T jet–wave regime in nonlinear (NL) and ensemble NL simulations. Ensemble simulations of the NL system (21) were performed by introducing in the mean equations in (21a), the ensemble average of $P_K(\mathbf{u}' \cdot \nabla \zeta')$, and $P_K(\mathbf{U} \cdot \nabla \zeta' + \mathbf{u}' \cdot \nabla \mathbf{Z})$ obtained from N_{ens} independent simulations of the perturbation NL equations in (21b) all with the same large-scale flow. The corresponding

results of the ensemble QL simulation (cf. Figs. 13a–d) differ from those of the ensemble NL simulation. The nonlinear term $(I - P_K)[\nabla \cdot (\mathbf{u}' \zeta')]$ is responsible for the difference between the NL and QL ensemble simulations, as shown in Fig. 13e–h. In this figure, an ensemble integration of the NL equations with this term absent is shown to produce results that are very close to the QL results.

When all waves with $|k_x| \geq 2$ are forced equally, as in the S3T examples discussed above, the eddy–eddy interactions are strong in the corresponding NL, resulting in a substantial modification of the spectrum of the eddy motions that is not reflected in S3T. To obtain correspondence, an effective stochastic forcing that parameterizes the absent eddy–eddy interactions is required in S3T (Constantinou et al. 2014).

Alternatively, when the term $(I - P_K)[\nabla \cdot (\mathbf{u}' \zeta')]$ is suppressed by choosing low forcing excitation, which results in weak modification of the spectrum of the incoherent component, agreement between NL and QL simulations is obtained. This is demonstrated in Fig. 14, in which we show results obtained with an approximate small-scale isotropic ring forcing:

$$\hat{Q}(\mathbf{k}) = \begin{cases} \frac{4\pi}{\log[(K_f + \delta K_f)/(K_f - \delta K_f)]} & \text{if } |k - K_f| \leq \delta K_f \text{ and } |k_x| > 1 \\ 0 & \text{if } |k - K_f| > \delta K_f \text{ or } |k_x| \leq 1, \end{cases} \quad (43)$$

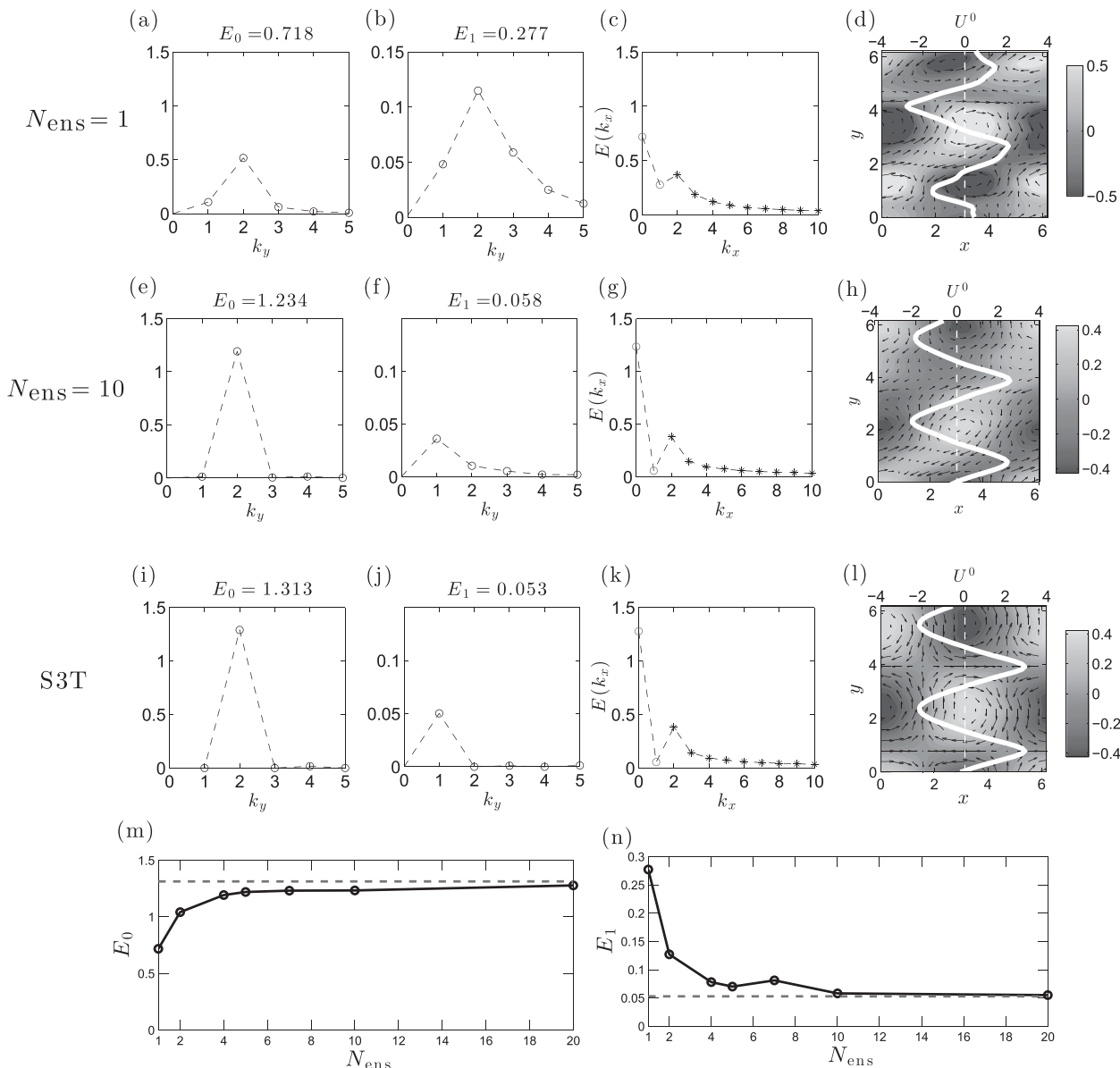


FIG. 12. (a)–(l) Structure of the mean flow in ensemble QL simulations as the number of ensemble members N_{ens} increases: (a)–(d) $N_{\text{ens}} = 1$, (e)–(h) $N_{\text{ens}} = 10$ at $\varepsilon/\varepsilon_c = 9$, and (i)–(l) the equilibrated mean flow from the S3T simulation at the same forcing amplitude (cf. Fig. 7). Shown are the k_y energy spectrum of (first column) the mean flow ($k_x = 0$), (second column) $k_x = 1$, and (third column) both the coherent-flow components $|k_x| \leq 1$ and the incoherent-flow components $|k_x| > 1$. (fourth column) Snapshots of the mean jet (thick line) and contour plot of the streamfunction of the $k_x = 1$ wave component. (m) The approach of the energy of the zonal flow E_0 , obtained in ensemble QL simulations as the number of ensemble members N_{ens} increases for the case $\varepsilon/\varepsilon_c = 9$. Dashed line marks the S3T prediction. (n) The approach of the wave component energy E_1 to the S3T predictions (dashed line). Convergence is achieved with $N_{\text{ens}} = 10$. Note that for small N_{ens} , fluctuations result in enhanced excitation of the $k_x = 1$ component. Parameters are as in previous simulations.

with $K_f = 10$, $\delta K_f = 1$, $r = 0.01$, and $\nu = 0$, as in Bakas and Ioannou (2014). With these parameters the S3T zonal jet equilibrium is stable to jet perturbations and unstable to $n_x = 1$ wave perturbations, and the resulting equilibrium state in NL has a wave $k_x = 1$ component in agreement with S3T predictions. Also the energetics of the mechanism of destabilization of the external $n_x = 1$

Rossby wave is partitioned between coherent and incoherent sources, consistent with the mechanism described in the previous sections.

It could be maintained that because isotropic ring forcing suppresses eddy–eddy interactions, the agreement between S3T and NL should be expected (cf. Bakas et al. 2015, their appendix C). This property

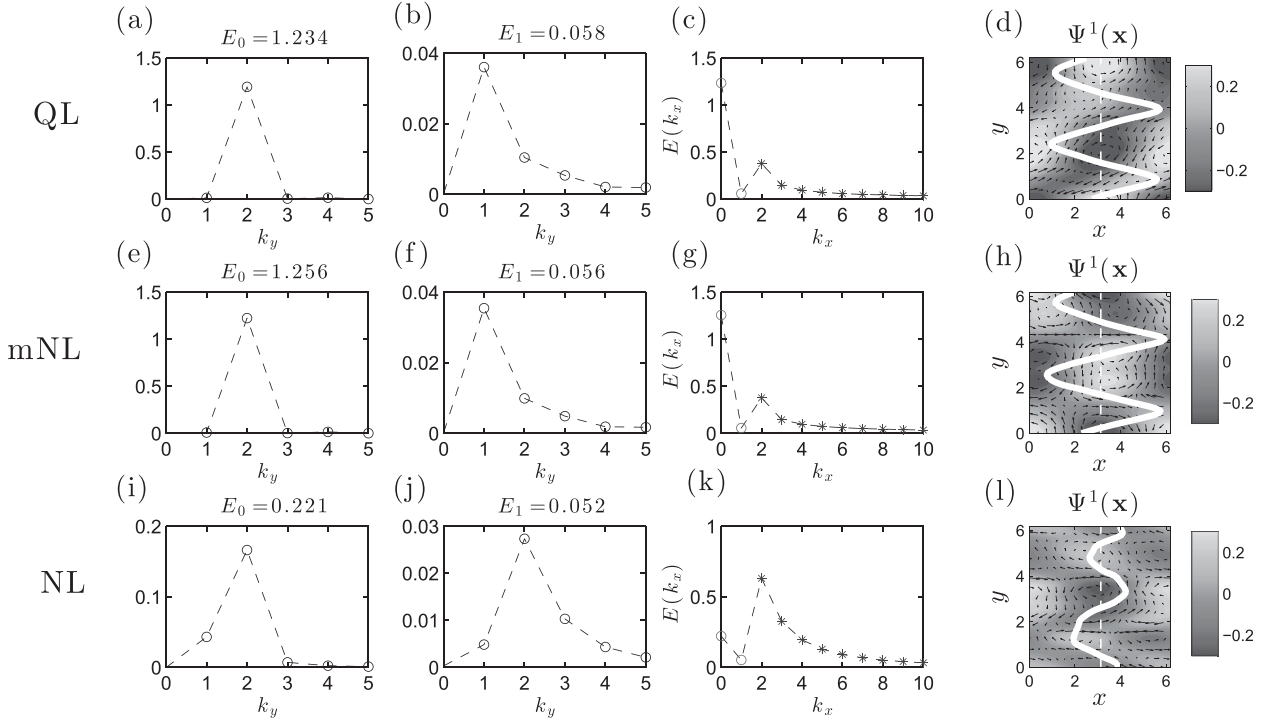


FIG. 13. (a)–(d) QL simulations, (e)–(h) modified NL simulations in which only the term $(I - P_K)[\nabla \cdot (\mathbf{u}'\zeta')]$ is removed, and (i)–(l) unmodified ensemble NL simulations, all with 10 ensemble members at $\varepsilon/\varepsilon_c = 9$. Shown are the k_y energy spectrum of (first column) the mean flow $k_x = 0$, (second column) the $k_x = 1$ component, and (third column) both the coherent flow components $|k_x| \leq 1$ and the incoherent flow components $k_x \geq 1$. (fourth column) Snapshots of the mean jet (thick line) and contour plot of the streamfunction of the wave component $k_x = 1$. Parameters are as in the other simulations. Note that the eddy–eddy interactions in NL lead in this particular example to an appreciable departure from the QL spectrum of the eddy components (i.e., wavenumbers $k_x \geq 2$) [cf. (c) and (k)]. This is because all the eddy components $k_x \geq 2$ are externally strongly forced (the dissipation has an e -folding of 40 days). This figure shows that the eddy–eddy nonlinearity is the source of the difference between the ensemble QL and the ensemble NL simulations.

follows from the fact that a barotropic fluid excited in an infinite channel with an isotropic ring forcing with spectrum $Q(\mathbf{k}) \propto \delta(|\mathbf{k}| - K_f)$ results in a nonlinear solution that, by itself, could never give rise to a jet. The emergence of jets under this forcing can only result from imposition of a separate perturbation, such as the jet perturbation that results in the S3T jet instability. As an example closer to physical reality, consider forcing of the form (25), which excites the zonal wavenumbers $8 \leq |k_x| \leq 14$, modeling baroclinic energy injection, and with linear damping for the incoherent scales $r = 1.5$ and $r_m = 0.1$ for the coherent scales, with corresponding e -folding times of 4 and 60 days, respectively. For these parameters, S3T theory predicts that the 5 jet equilibrium at $\varepsilon = 0.830$ is stable to both jet and $n_x = 1$ wave perturbations, and consequently S3T theory predicts that QL and NL simulations should show suppressed energy in the $k_x = 1$ coherent wave component. Good agreement between QL and NL is found in the channel, as shown in Fig. 15. It is interesting to note that, while the jet in the NL simulation has the structure predicted by the S3T, its

amplitude is reduced, consistent with a component of the eddy–eddy interactions acting as diffusion on the mean jet.

9. Conclusions

Large-scale coherent structures, such as jets, meandering jets, and waves embedded in jets are characteristic features of turbulence in planetary atmospheres. While conservation of energy and enstrophy in inviscid 2D turbulence predicts spectral evolution leading to concentration of energy at large scales, these considerations cannot predict the phase of the spectral components and therefore cannot address the central question of the organization of the energy into specific structures such as jets and the coherent component of planetary-scale waves. To study structure formation, additional aspects of the dynamics beyond conservation principles must be incorporated in the analysis. For this purpose, SSD models have been developed and used to study the formation of coherent structure in

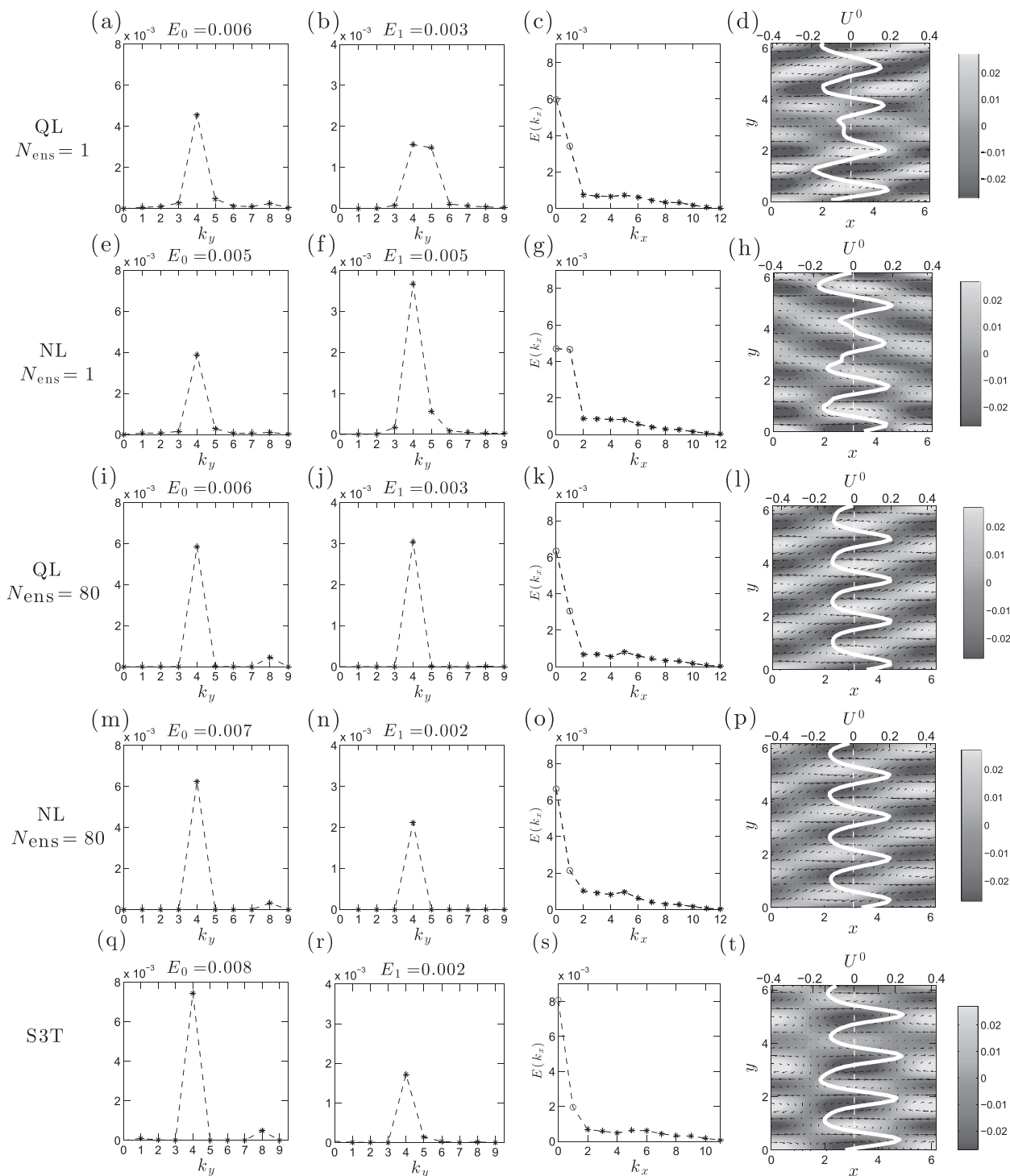


FIG. 14. Comparison among QL and NL simulations with ensemble members (a)–(h) $N_{ens} = 1$, (i)–(p) $N_{ens} = 80$, and (q)–(t) S3T simulation. The S3T state in this example predicts a jet component and a $k_x = 1$ component, and this is reflected in both QL and NL ensemble simulations, as revealed by the k_y energy spectrum of (first column) the respective mean flow ($k_x = 0$), (second column) the $k_x = 1$ component, and (third column) the k_x energy spectrum. (fourth column) Snapshots of the mean flow (thick line) and contour plot of the streamfunction of the wave component $k_x = 1$. Simulations with isotropic forcing at total wavenumber $K_f = 10$ [cf. (43)] with $\varepsilon = 4.2 \times 10^{-4}$, linear damping coefficient $r = 0.01$, and $\nu = 0$.

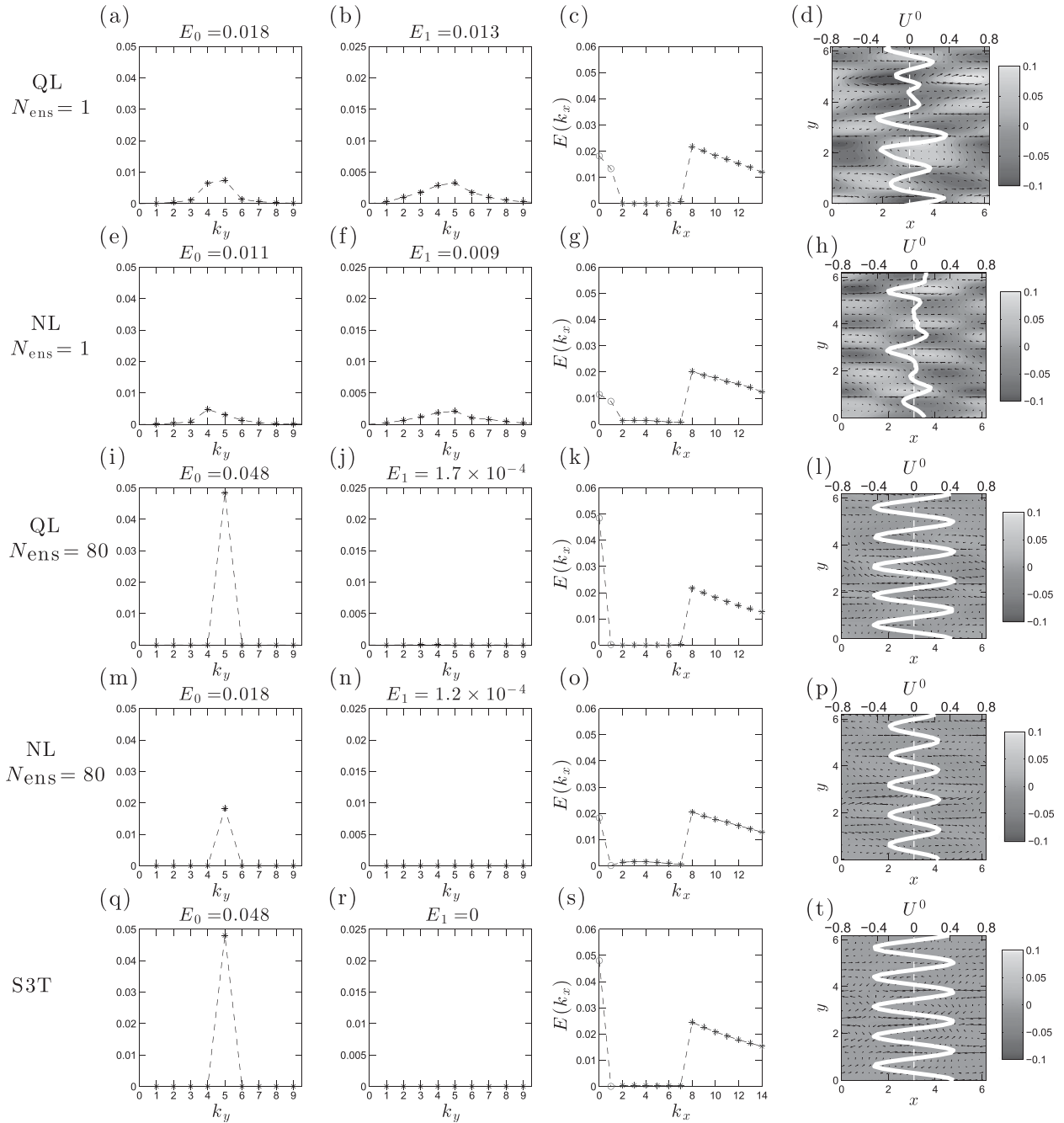


FIG. 15. Comparison among QL and NL simulations with ensemble members (a)–(h) $N_{\text{ens}} = 1$, (i)–(p) $N_{\text{ens}} = 80$, and (q)–(t) S3T simulation. The S3T state in this example predicts only a jet component and no $k_x = 1$ component, and this is reflected in both QL and NL ensemble simulations, as revealed by the k_y energy spectrum of (first column) the respective mean flow ($k_x = 0$), (second column) the $k_x = 1$ component, and (third column) the k_x energy spectrum. (fourth column) Snapshots of the mean flow (thick line) and contour plot of the streamfunction of the wave component $k_x = 1$. Simulations with the anisotropic forcing spectrum (25) at $\varepsilon = 0.830$ with zonal wavenumbers $8 \leq |k_x| \leq 14$ being forced. Mean linear damping coefficient is $r_m = 0.1$, and linear damping coefficient of the incoherent flow is $r = 1.5$ and $\nu = 0$.

planetary-scale turbulence. In this work, an SSD model was formulated for the purpose of studying the regime of coexisting jets and waves. In this model, a separation in zonal Fourier modes is made by projection in order to

separate a coherent structure equation, in which only the gravest zonal harmonics are retained, from the remaining spectrum, which is assumed to be incoherent and gives rise to the ensemble-mean second-order

statistics associated with the incoherent turbulence. This second-order SSD model is closed by a stochastic forcing parameterization that accounts for both the neglected nonlinear dynamics of the small scales as well as the forcing maintaining the turbulence. The equation for the large scales retains its nonlinearity and its interaction through Reynolds stress with the eddies.

In this model, jets form as instabilities and equilibrate nonlinearly at finite amplitude. A stable mode of the Rossby wave spectrum associated with these jets is destabilized for sufficiently strong forcing by interaction with eddy Reynolds stresses. This destabilization is found to have, in some cases, the remarkable property of resulting from destabilization of the retrograde Rossby wave to mean jet interaction by structural modification of this damped mode arising from its interaction with the incoherent turbulence, thereby transforming it into an unstable mode of the mean jet. In other cases, comparable contributions are found from direct forcing by the Reynolds stresses, as in S3T instability with projections at $K = 0$, and induced jet–wave interaction, as in traditional hydrodynamic instability. This synergistic interaction provides a powerful new mechanism for maintaining planetary waves that will be the subject of further investigation.

Acknowledgments. We thank Nikolaos Bakas for useful discussions on the energetics of the equations in spectral space. We also thank the anonymous reviewers for their comments that led to improvement of the paper. N.C.C. would like to thank Prof. Georgios Georgiou for his hospitality and support during the summer of 2015 at the University of Cyprus. B.F.F. was supported by NSF AGS-1246929. N.C.C. was partially supported by the NOAA Climate and Global Change Postdoctoral Fellowship Program, administered by UCAR's Visiting Scientist Programs.

REFERENCES

- Ait-Chaalal, F., T. Schneider, B. Meyer, and J. B. Marston, 2016: Cumulant expansions for atmospheric flows. *New J. Phys.*, **18**, 025019, doi:10.1088/1367-2630/18/2/025019.
- Bakas, N. A., and P. J. Ioannou, 2013a: Emergence of large scale structure in barotropic β -plane turbulence. *Phys. Rev. Lett.*, **110**, 224501, doi:10.1103/PhysRevLett.110.224501.
- , and —, 2013b: On the mechanism underlying the spontaneous emergence of barotropic zonal jets. *J. Atmos. Sci.*, **70**, 2251–2271, doi:10.1175/JAS-D-12-0102.1.
- , and —, 2014: A theory for the emergence of coherent structures in beta-plane turbulence. *J. Fluid Mech.*, **740**, 312–341, doi:10.1017/jfm.2013.663.
- , N. C. Constantinou, and P. J. Ioannou, 2015: S3T stability of the homogeneous state of barotropic beta-plane turbulence. *J. Atmos. Sci.*, **72**, 1689–1712, doi:10.1175/JAS-D-14-0213.1.
- Baldwin, M. P., P. B. Rhines, H.-P. Huang, and M. E. McIntyre, 2007: The jet-stream conundrum. *Science*, **315**, 467–468, doi:10.1126/science.1131375.
- Berloff, P., I. Kamenkovich, and J. Pedlosky, 2009: A mechanism of formation of multiple zonal jets in the oceans. *J. Fluid Mech.*, **628**, 395–425, doi:10.1017/S0022112009006375.
- Bernstein, J., and B. F. Farrell, 2010: Low-frequency variability in a turbulent baroclinic jet: Eddy–mean flow interactions in a two-level model. *J. Atmos. Sci.*, **67**, 452–467, doi:10.1175/2009JAS3170.1.
- Bouchet, F., and A. Venaille, 2012: Statistical mechanics of two-dimensional and geophysical flows. *Phys. Rep.*, **515**, 227–295, doi:10.1016/j.physrep.2012.02.001.
- , C. Nardini, and T. Tangarife, 2013: Kinetic theory of jet dynamics in the stochastic barotropic and 2D Navier–Stokes equations. *J. Stat. Phys.*, **153**, 572–625, doi:10.1007/s10955-013-0828-3.
- Cai, M., and M. Mak, 1990: Symbiotic relation between planetary and synoptic-scale waves. *J. Atmos. Sci.*, **47**, 2953–2968, doi:10.1175/1520-0469(1990)047<2953:SRBPAS>2.0.CO;2.
- Connaughton, C. P., B. T. Nadiga, S. V. Nazarenko, and B. E. Quinn, 2010: Modulational instability of Rossby and drift waves and generation of zonal jets. *J. Fluid Mech.*, **654**, 207–231, doi:10.1017/S0022112010000510.
- Constantinou, N. C., 2015: Formation of large-scale structures by turbulence in rotating planets. Ph.D. thesis, National and Kapodistrian University of Athens, 204 pp. [Available online at <http://www.didaktorika.gr/eadd/handle/10442/35501?locale=en>.]
- , B. F. Farrell, and P. J. Ioannou, 2014: Emergence and equilibration of jets in beta-plane turbulence: Applications of stochastic structural stability theory. *J. Atmos. Sci.*, **71**, 1818–1842, doi:10.1175/JAS-D-13-076.1.
- Cross, M., and H. Greenside, 2009: *Pattern Formation and Dynamics in Nonequilibrium Systems*. Cambridge University Press, 552 pp.
- Dritschel, D. G., and M. E. McIntyre, 2008: Multiple jets as PV staircases: The Phillips effect and the resilience of eddy-transport barriers. *J. Atmos. Sci.*, **65**, 855–874, doi:10.1175/2007JAS2227.1.
- Farrell, B. F., and P. J. Ioannou, 2002: Perturbation growth and structure in uncertain flows. Part II. *J. Atmos. Sci.*, **59**, 2647–2664, doi:10.1175/1520-0469(2002)059<2647:PGASIU>2.0.CO;2.
- , and —, 2003: Structural stability of turbulent jets. *J. Atmos. Sci.*, **60**, 2101–2118, doi:10.1175/1520-0469(2003)060<2101:SSOTJ>2.0.CO;2.
- , and —, 2007: Structure and spacing of jets in barotropic turbulence. *J. Atmos. Sci.*, **64**, 3652–3665, doi:10.1175/JAS4016.1.
- , and —, 2008: Formation of jets by baroclinic turbulence. *J. Atmos. Sci.*, **65**, 3353–3375, doi:10.1175/2008JAS2611.1.
- , and —, 2009a: Emergence of jets from turbulence in the shallow-water equations on an equatorial beta plane. *J. Atmos. Sci.*, **66**, 3197–3207, doi:10.1175/2009JAS2941.1.
- , and —, 2009b: A stochastic structural stability theory model of the drift wave–zonal flow system. *Phys. Plasmas*, **16**, 112903, doi:10.1063/1.3258666.
- , and —, 2009c: A theory of baroclinic turbulence. *J. Atmos. Sci.*, **66**, 2444–2454, doi:10.1175/2009JAS2989.1.
- , and —, 2012: Dynamics of streamwise rolls and streaks in turbulent wall-bounded shear flow. *J. Fluid Mech.*, **708**, 149–196, doi:10.1017/jfm.2012.300.
- , and —, 2016: Statistical state dynamics: A new perspective on turbulence in shear flow. *Zonal Jets*, B. Galperin and P. L. Read, Eds., Cambridge University Press, in press. [Available online at <http://arxiv.org/abs/1412.8290>.]

- Fjørtoft, R., 1953: On the changes in the spectral distribution of kinetic energy for two-dimensional, nondivergent flow. *Tellus*, **5A**, 225–230, doi:10.1111/j.2153-3490.1953.tb01051.x.
- Frisch, U., 1995: *Turbulence: The Legacy of A. N. Kolmogorov*. Cambridge University Press, 312 pp.
- Gill, A. E., 1974: The stability of planetary waves on an infinite beta-plane. *Geophys. Astrophys. Fluid Dyn.*, **6**, 29–47, doi:10.1080/03091927409365786.
- Kasahara, A., 1980: Effect of zonal flows on the free oscillations of a barotropic atmosphere. *J. Atmos. Sci.*, **37**, 917–929, doi:10.1175/1520-0469(1980)037<0917:EOZFOT>2.0.CO;2.
- Lorenz, E. N., 1972: Barotropic instability of Rossby wave motion. *J. Atmos. Sci.*, **29**, 258–269, doi:10.1175/1520-0469(1972)029<0258:BIORWM>2.0.CO;2.
- Manfroi, A. J., and W. R. Young, 1999: Slow evolution of zonal jets on the beta plane. *J. Atmos. Sci.*, **56**, 784–800, doi:10.1175/1520-0469(1999)056<0784:SEOZJO>2.0.CO;2.
- Marston, J. B., 2012: Planetary atmospheres as nonequilibrium condensed matter. *Annu. Rev. Condens. Matter Phys.*, **3**, 285–310, doi:10.1146/annurev-conmatphys-020911-125114.
- , E. Conover, and T. Schneider, 2008: Statistics of an unstable barotropic jet from a cumulant expansion. *J. Atmos. Sci.*, **65**, 1955–1966, doi:10.1175/2007JAS2510.1.
- , G. P. Chini, and S. M. Tobias, 2016: The generalized quasi-linear approximation: Application to zonal jets. 5 pp. [Available online at <http://arxiv.org/abs/1601.06720>.]
- Miller, J., 1990: Statistical mechanics of Euler equations in two dimensions. *Phys. Rev. Lett.*, **65**, 2137–2140, doi:10.1103/PhysRevLett.65.2137.
- Parker, J. B., 2014: Zonal flows and turbulence in fluids and plasmas. Ph.D. thesis, Princeton University, 157 pp. [Available online at <http://arks.princeton.edu/ark:/88435/dsp01h989r543m>.]
- , and J. A. Krommes, 2013: Zonal flow as pattern formation. *Phys. Plasmas*, **20**, 100703, doi:10.1063/1.4828717.
- , and —, 2014: Generation of zonal flows through symmetry breaking of statistical homogeneity. *New J. Phys.*, **16**, 035006, doi:10.1088/1367-2630/16/3/035006.
- Qin, J., and W. A. Robinson, 1992: Barotropic dynamics of interactions between synoptic and low-frequency eddies. *J. Atmos. Sci.*, **49**, 71–79, doi:10.1175/1520-0469(1992)049<0071:BDOIBS>2.0.CO;2.
- Rhines, P. B., 1975: Waves and turbulence on a beta-plane. *J. Fluid Mech.*, **69**, 417–433, doi:10.1017/S0022112075001504.
- Robert, R., and J. Sommeria, 1991: Statistical equilibrium states for two-dimensional flows. *J. Fluid Mech.*, **229**, 291–310, doi:10.1017/S0022112091003038.
- Robinson, W. A., 1991: The dynamics of low-frequency variability in a simple model of the global atmosphere. *J. Atmos. Sci.*, **48**, 429–441, doi:10.1175/1520-0469(1991)048<0429:TDOLFV>2.0.CO;2.
- Salby, M. L., 1982: A ubiquitous wavenumber-5 anomaly in the Southern Hemisphere during FGGE. *Mon. Wea. Rev.*, **110**, 1712–1721, doi:10.1175/1520-0493(1982)110<1712:AUWAIT>2.0.CO;2.
- Sánchez-Lavega, A., and Coauthors, 2014: The long-term steady motion of Saturn’s hexagon and the stability of its enclosed jet stream under seasonal changes. *Geophys. Res. Lett.*, **41**, 1425–1431, doi:10.1002/2013GL059078.
- Scott, R. K., and D. G. Dritschel, 2012: The structure of zonal jets in geostrophic turbulence. *J. Fluid Mech.*, **711**, 576–598, doi:10.1017/jfm.2012.410.
- Srinivasan, K., and W. R. Young, 2012: Zonostrophic instability. *J. Atmos. Sci.*, **69**, 1633–1656, doi:10.1175/JAS-D-11-0200.1.
- Tangarife, T., 2015: Kinetic theory and large deviations for the dynamics of geophysical flows. Ph.D. thesis, École Normale Supérieure de Lyon, 186 pp. [Available online at <http://www.theses.fr/2015ENSL1037>.]
- Thomas, V., B. K. Lieu, M. R. Jovanović, B. F. Farrell, P. J. Ioannou, and D. F. Gayme, 2014: Self-sustaining turbulence in a restricted nonlinear model of plane Couette flow. *Phys. Fluids*, **26**, 105112, doi:10.1063/1.4898159.
- , B. F. Farrell, P. J. Ioannou, and D. F. Gayme, 2015: A minimal model of self-sustaining turbulence. *Phys. Fluids*, **27**, 105104, doi:10.1063/1.4931776.
- Tobias, S. M., and J. B. Marston, 2013: Direct statistical simulation of out-of-equilibrium jets. *Phys. Rev. Lett.*, **110**, 104502, doi:10.1103/PhysRevLett.110.104502.
- Vasavada, A. R., and A. P. Showman, 2005: Jovian atmospheric dynamics: An update after *Galileo* and *Cassini*. *Rep. Prog. Phys.*, **68**, 1935–1996, doi:10.1088/0034-4885/68/8/R06.